

**Fabrication and Simulation of
PICT/PAN Based Nonwoven Nano-
Fabric for Guided Bone Regeneration**



By

Uzair Rafique

**School of Chemical and Materials Engineering
National University of Sciences and Technology**

2023

Fabrication and Simulation of PICT/PAN Based Nonwoven Nano- Fabric for Guided Bone Regeneration



Name: Uzair Rafique

Reg. No.: Fall-2019-MS-PSE-02-00000318365

**This work is submitted as a partial fulfillment of the
requirement for the degree of**

MS in Process Systems Engineering

Supervisor Name: Dr. Umair Sikander

School of Chemical and Materials Engineering (SCME)

National University of Sciences and Technology (NUST)

H-12, Islamabad, Pakistan

JUNE 2023



THESIS ACCEPTANCE CERTIFICATE

Certified that final copy of MS thesis written by Mr **Uzair Rafique** (Registration No 00000318365), of School of Chemical & Materials Engineering (SCME) has been vetted by undersigned, found complete in all respects as per NUST Statues/Regulations, is free of plagiarism, errors, and mistakes and is accepted as partial fulfillment for award of MS degree. It is further certified that necessary amendments as pointed out by GEC members of the scholar have also been incorporated in the said thesis.

Signature: _____

Name of Supervisor: **Dr Umair Sikandar**

Date: _____

13-09-23

Signature (HOD): _____

Date: _____

4/10/23

Signature (Dean/Principal): _____

Date: _____

4.10.23

E/Ver. 1

Form TH-1

National University of Sciences & Technology (NUST)
MASTER'S THESIS WORK
Formulation of Guidance and Examination Committee



Name: UZAIR RAFIQUE
00000318365

NUST Reg No: Fall2019-MS-PSE-02-

Department: SCME

Specialization: Process Systems Engineering
CGPA: 3.00

Credit Hour Completed (21) 24

Course Work Completed

S/No	Code	Title	Core/Elective	CH	Grade
1	PSE-801	Process System Theory	Core	03	B
2	PSE-852	Process Modeling and Simulation	Core	03	C+
3	PSE-802	Optimization and Decision Analysis	Core	03	B
4	PSE-823	Advance Process Dynamics & Controls	Core	03	B+
5	<u>TEE-820</u>	Process Intensification	Elective	03	B
6	<u>CSE-841</u>	Computational Fluid Dynamic	Elective	03	B
7	<u>EME-921</u>	Momentum Heat & Mass Transfer in Chem Engg.	Elective	03	B
8	<u>RM-898</u>	Research Methodology	<u>Additional</u>	<u>02</u>	<u>@</u>
9	ENE-809	Wastewater Treatment & Design	Elective	03	B

Exam Br
28/9/19

Date _____
Thesis Committee

Student's Signature:

- Name: Dr. Umair Sikander (Supervisor)
Department: SCME
- Name: Dr. Bilal Khan Niazi (Co-Supervisor)
Department: SCME
- Name: Dr. Salman Raza Naqvi
Department: SCME
- Name: Dr. Zartasha Mustansar
Department: RCMS
- Name: Dr. Muhammad Oamar Khan (External)
National Textile University, Karachi

Signature: _____

Signature: _____

Signature: _____

Signature: _____

Signature: _____

Date: 28/9/21

Signature Of Head of Department

APPROVAL

Date: 28-9-21

Signature: _____

Signature: _____

Signature of Dean/Principal

Distribution

- 1x copy to Exam Branch, HQ NUST
- 1x copy to PGP Date, HQ NUST
- 1x copy to Exam branch, respective institute



Form: TH-01

National University of Sciences & Technology (NUST)

MASTER'S THESIS WORK

We hereby recommend that the dissertation prepared under our supervision by

Regn No & Name: 00000318365 Uzair Rafique


Title: Fabrication and Simulation of PICT/PAN Based Nonwoven Nano-Fabric for Guided Bone Regeneration.

Presented on: 10 Aug 2023 at: 1430 hrs in SCME (Seminar Hall)

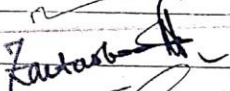
Be accepted in partial fulfillment of the requirements for the award of Master of Science degree in Process Systems Engineering.

Guidance & Examination Committee Members


Name: Dr M. Qamar Khan

Signature: 

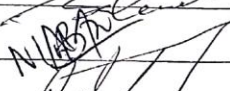
Name: Dr Zartasha Mustansar

Signature: 

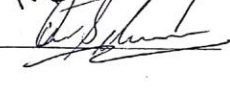
Name: Dr Salman Raza Naqvi

Signature: 

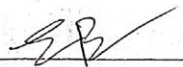
Name: Dr M Bilal Khan Niazi (Co-Supervisor)

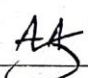
Signature: 

Supervisor's Name: Dr Umair Sikandar

Signature: 

Dated: _____


Head of Department
Date 31/8/23


Dean/Principal
Date 4.9.2023

School of Chemical & Materials Engineering (SCME)

Dedication

To the one who reminded me that it's never too late to change course and encouraged me to explore new directions. Thank you for your role as a beacon of guidance on my journey towards a promising future.

Acknowledgements

"The author expresses profound gratitude to Almighty Allah, for without His graces and blessings, this study would not have been possible. The author would also like to extend sincere appreciation to the supervisor, advisory committee members, friends and family who contributed to this research. Their unwavering support has been invaluable throughout this journey."

Uzair rafique

Abstract

This master's thesis presents a comprehensive study on the development of a non-woven coaxial nanofibrous polymeric scaffold for potential use in hard tissue engineering and regenerative applications, specifically for bone regeneration. The main objective was to create a controlled drug delivery system that meets the required standards for bone regeneration applications. Various scaffolding techniques were investigated, and electrospinning was chosen as the preferred method due to its advantages such as higher product selectivity, cost-effectiveness, high production rate, simplicity, stability, and compatibility with bone tissue.

The scaffold was designed to have well-defined core and shell structures, with ZnO/HA and SiO₂/CaO nanoparticles incorporated in the core and shell respectively. Biocompatible, non-toxic, high-strength polymers, namely PICT and PAN, were used to construct the shell and core, ensuring mechanical stability, biocompatibility, and desired physiochemical properties such as hydrophobicity. The scaffold's mechanical properties, including tensile strength and elongation, were carefully evaluated to ensure its ability to withstand stresses and provide support when implanted in bone.

Three scaffolds with different percentages of bioceramic nanoparticles were fabricated and compared based on various factors such as structural properties, surface morphology, tensile strength, elongation, cell survival, and wetting behavior. Scaffold B emerged as the most feasible option, exhibiting excellent biocompatibility, supporting high cell survival (85%), and possessing a desired water contact angle (127.2°) to maintain scaffold strength for guided bone regeneration. Scaffold B showed a tensile strength of 1.7 MPa and an elongation of 7%, making it suitable for guided bone regeneration.

The study emphasized the importance of the scaffold's structure and properties, including fiber diameter distribution, porosity, hydrophobicity, cell survival, and interconnectivity, in its effectiveness for bone regeneration. The scaffold's structure influenced its strength, cell infiltration, and mineral and oxygen transportation. The electrospinning process was optimized to produce a scaffold with the desired structure.

Furthermore, simulation was conducted to investigate the behavior of single fibers under stress. ABAQUS software was used for FEM analysis, and future work involves using simulation to validate experimental results and predict scaffold behavior with different compositions. This will further optimize scaffold properties for specific applications and impact tissue regeneration.

The developed electrospun polymeric scaffold exhibits great potential for tissue engineering and bone regeneration. Further research and development can optimize its properties and evaluate its effectiveness *in vivo*. With continued progress, this scaffold holds promise for a wide range of applications, including wound healing and bone tissue engineering.

Table of Contents

DEDICATION	I
ACKNOWLEDGEMENTS	II
ABSTRACT	III
LIST OF FIGURES	VIII
LIST OF TABLES	IX
CHAPTER 1	1
INTRODUCTION	1
1.2 SCAFFOLDS FOR CONTROLLED DRUG DELIVERY	2
1.3 INTRODUCTION TO NON-WOVEN:	2
1.4 RESEARCH AIM 1	3
1.5 RESEARCH AIM 2	4
1.6 RESEARCH AIM 3	5
CHAPTER 2	6
LITERATURE REVIEW	6
2.1 BONE STRUCTURE AND FUNCTION	6
2.1.1 Introduction:	6
2.1.2 Classification of Bone:	6
2.1.3 Cortical and Trabecular Bone:	7
2.1.4 Bone Matrix:	8
2.1.5 Woven and Lamellar Bones:	9
2.1.6 Bone Cells and Their Functions:	10
2.1.7 Periosteum and Endosteum:	12
2.2 BONE MORPHOGENESIS AND REGENERATION	12
2.2.1 Bone Development and Regeneration:	12
2.2.2 Fracture Healing:	14
2.2.3 BMPs in Skelton Development and Fracture Healing:	15

2.3 BONE REGENERATION AND CLINICAL TREATMENTS	17
2.3.1 Clinical Needs for Bone Regeneration:	17
2.3.2 Clinical Bone Repair Strategies:.....	18
2.3.3 BMPs in clinical practice:.....	19
2.3.4 Drawbacks and Limitations of BMPs:.....	19
2.4 RESEARCH APPROACHES FOR BONE REGENERATION:	20
2.4.1 Tissue Engineering/Regenerative Medicine (TE/RM):	20
2.4.2 Scaffolds:	21
2.4.3 Cell Sourcing and Delivery:	22
CHAPTER 3	24
OVERVIEW OF DEVELOPED METHOD AND MODELS	24
3.1 ELECTROSPINNING:	24
3.1.1 Electrospinning Working Principle:	26
3.1.2 Process Parameters:	27
3.2 FREEZE DRYING:	31
3.2.1 Drawbacks and Limitations of Freeze Drying:.....	32
3.3 BIO-PRINTING:	33
3.3.1 Bio-Printing Process:	33
3.3.1.1 PRE-PRINTING:	33
3.3.2 Parametric Considerations:.....	35
3.3.3 Advantages of Bio Printing:	36
3.3.4 Drawbacks & Limitations of Bio-Printing:	37
3.4 : SIMULATION:.....	37
3.4.1 Simulation Process Steps:.....	37
3.4.2 Finite Element Method (FEM):	38
3.4.3 Finite Volume Method (FVM):	38
3.4.4 Boundary Element Method (BEM):	39
3.4.5 Finite Difference Method (FDM):.....	39
CHAPTER 4	40
MATERIALS AND METHODS.....	40
4.1 PROBLEM STATEMENT:	40
4.2 MATERIALS:	41

4.3 METHODOLOGY:.....	46
4.4 FABRICATION OF CORE AND SHELL NANOFIBERS:.....	47
4.4.1 1 st coaxial Nano fibrous Scaffold:.....	48
4.4.2 2 nd coaxial Nano fibrous Scaffold:	50
4.4.3 3 rd coaxial Nanofibrous Scaffold:.....	54
4.5 CHARACTERIZATION AND TESTING	56
4.5.1 Introduction to FTIR:.....	56
4.5.2 Introduction to TEM:.....	57
4.5.3 Introduction to Water Contact Angle:	58
4.5.4 Introduction to SEM:	60
4.6 MODELING & SIMULATION USING FEM:	61
4.6.1 Simulation Process Steps:.....	62
4.6.2 Modeling of Scaffold:.....	63
CHAPTER 5	68
RESULT AND DISCUSSION	68
5.1 INVITRO CYTOTOXICITY:.....	68
5.2 MORPHOLOGY OF NANOFIBERS:	70
5.2.1 SEM:	70
5.2.2 TEM:.....	71
5.3 TENSILE TESTING:	72
5.4 WATER CONTACT ANGLE:	74
5.5 FTIR SPECTRA:	76
5.6 FEM RESULTS:.....	78
CONCLUSIONS	81
RECOMMENDATIONS	83
REFERENCES	84

List of Figures

Figure 1.1: Areas of Application of Non-Woven Nano Fiber	3
Figure 2.1: Primary Components of bone.....	7
Figure 2.2: Relationship between Trabecular and cortical bone.....	8
Figure 2.3: Woven Bone and Lamellar Bone	10
Figure 2.4: Cell types and Functions	11
Figure 2.5: Structure and Position of the endosteum and periosteum	12
Figure 2.6: Osteocalcin functions	16
Figure 2.7: Biological components to the site of injury.....	22
Figure 3.1: Scheme of Electrospinning Working	26
Figure 3.2: Freeze Drying Process.....	32
Figure 3.3: Bio Printing Process	35
Figure 3.4: CFD-Simulation Process	38
Figure 4.1: Scheme of Development of Nano Fibrous Scaffold.....	46
Figure 4.2	64
Figure 4.3	64
Figure 4.4	65
Figure 4.5	65
Figure 4.6	66
Figure 4.7	66
Figure 4.8	67
Figure 4.9	67
Figure 5.1: Images For Invitro Study.....	69
Figure 5.2: Image Of Cell Survival Percentage	70
Figure 5.3: SEM Images Of Nano Fibrous Scaffolds	71
Figure 5.4: TEM Images Of Scaffolds.....	72
Figure 5.5: Tensile Strength And Elongation Graph	74
Figure 5.6: Graph Image Of Wettability Behavior	76
Figure 5.7: FTIR Spectra	78
Figure 5.8	79
Figure 5.9	79
Figure 5.10:stress components along respective direction vectors	80

List of Tables

Table 2.1: The Cleveland Clinic's Bone Augmentation Success Rate & Frequency. .	18
Table 4.1: Properties of PAN.....	41
Table 4.2: Properties of HA.....	43
Table 4.3: Properties of CaO.....	44
Table 4.4: Properties of SiO ₂	45
Table 4.5: Properties ZnO.....	46
Table 4.6: Composition of all Scaffolds.....	47
Table 4.7: Composition of 1st shell solution.....	49
Table 4.8: Composition of 1st core solution.....	50
Table 4.9: Composition of 2nd Shell Solution.....	52
Table 4.10: Composition of 2nd Core Solution.....	53
Table 4.11: Composition of 3rd Shell Solution.....	55
Table 4.12: Composition of 3rd Core Solution.....	56

List of Abbreviations

PCL	Polycaprolactone
ECM	Extracellular Matrix
PLGA	Poly(lactic-co-glycolic acid)
PEG	Polyethylene Glycol
FTIR	Fourier Transform Infrared Spectroscopy
SEM	Scanning Electron Microscope
TEM	Transmission Electron Microscope
FEM	Finite Element Method
FEA	Finite Element Analysis
TFA	Trifluoroacetic Acid
HA	Hydroxyapatite
CaO	Calcium Oxide
ZnO	Zinc Oxide
SiO ₂	Silicon Dioxide
PICT	Poly(1,4-cyclohexanedimethylene isosorbide terephthalate)
PAN	Polyacrylonitrile
DMF	Dimethylformamide
GBR	Guided Bone Regeneration
TE/RM	Tissue Engineering / Regenerative Medicine
FDA	Food and Drug Administration
BTE	Bone Tissue Engineering

Chapter 1

Introduction

1.1 Introduction

Bone is a rigid, calcified connective tissue that provides structural support for the body, protects internal organs, stores minerals such as calcium and phosphorus, and produces blood cells [1]. The human skeletal system is made up of 206 bones of different shapes and sizes that are connected by joints, ligaments, and cartilage [2].

Bones play a vital role in the body, as they provide support and protection for vital organs, aid in movement and locomotion, and help to maintain the body's mineral balance. They also serve as a storage reservoir for important minerals such as calcium, which is essential for many physiological processes [3].

Bone is a type of tissue that makes up the skeletal system. However, it is true that bone is one of the most commonly transplanted tissues, after blood.

When bone tissue is damaged or lost due to injury, disease, or aging, the body has natural mechanisms for repairing or regrowing it. However, in some cases, medical interventions may be necessary to help speed up the process. This process is known as bone regeneration and involves the growth and differentiation of bone cells, as well as the deposition of new bone matrix.

Various techniques can be used to promote bone regeneration, including bone grafts, the use of growth factors or stem cells, and the application of biomaterials or scaffolds that provide a framework for new bone growth. The development of new treatments for bone regeneration is an area of active research, as it has the potential to help individuals with a variety of bone disorders and injuries, including fractures, osteoporosis, and bone cancer [4].

Electrospun non-woven nanofibers have shown promise in the field of bone regeneration. These nanofibers are made from polymer solutions that are spun into fibers using an electrostatic field. The resulting non-woven mesh has a high surface area and porosity, which can support the attachment, proliferation, and differentiation of bone cells [5]. Electrospun nanofibers have several advantages for bone

regeneration, including their ability to mimic the natural extracellular matrix of bone tissue, their high surface area, and their tunable mechanical properties [6].

These fibers have the high strength required for guided bone growth, and they can also be loaded with growth factors, bioceramic, or other drugs to enhance their Research in this field is ongoing, and Electrospun nanofibers are being studied for their potential use in a variety of bone regeneration applications.

1.2 Scaffolds for Controlled Drug Delivery

One approach for controlled drug delivery using scaffolds is to incorporate the drug into the scaffold material itself. For example, a drug can be mixed with a polymer solution and then the solution can be cast into the desired scaffold shape, allowing the drug to be released slowly over time [7].

Regardless of the approach used, the scaffold can be designed to release the drug in a controlled manner, either by diffusion or degradation of the scaffold material. By controlling the release rate, the drug can be delivered over an extended period of time, reducing the need for frequent dosing, and improving patient compliance [8].

Our prime objective is to develop a non-woven, coaxial nano fabric incorporated with bioceramic to enhance bone regeneration capabilities in humans. In order to facilitate guided bone regeneration(GBR), this nanofiber must be strong enough to support broken bone/bone fractures [9].

1.3 Introduction to Non-Woven:

Nonwoven fabrics are engineered textiles made by bonding or interlocking fibers together without the need for weaving or knitting. Nonwovens can be made from a variety of natural or synthetic fibers, such as polyester, polypropylene, polyacrylonitrile, cotton, and nylon, among others. The fibers are typically randomly arranged, creating a porous material that can have varying degrees of thickness, strength, and texture.

Nonwoven fabrics are commonly used in products such as face masks, surgical gowns, diapers, wipes, insulation, roofing materials, and more. They have a wide

range of applications in various industries, including medical, hygiene, filtration, automotive, construction, and more.

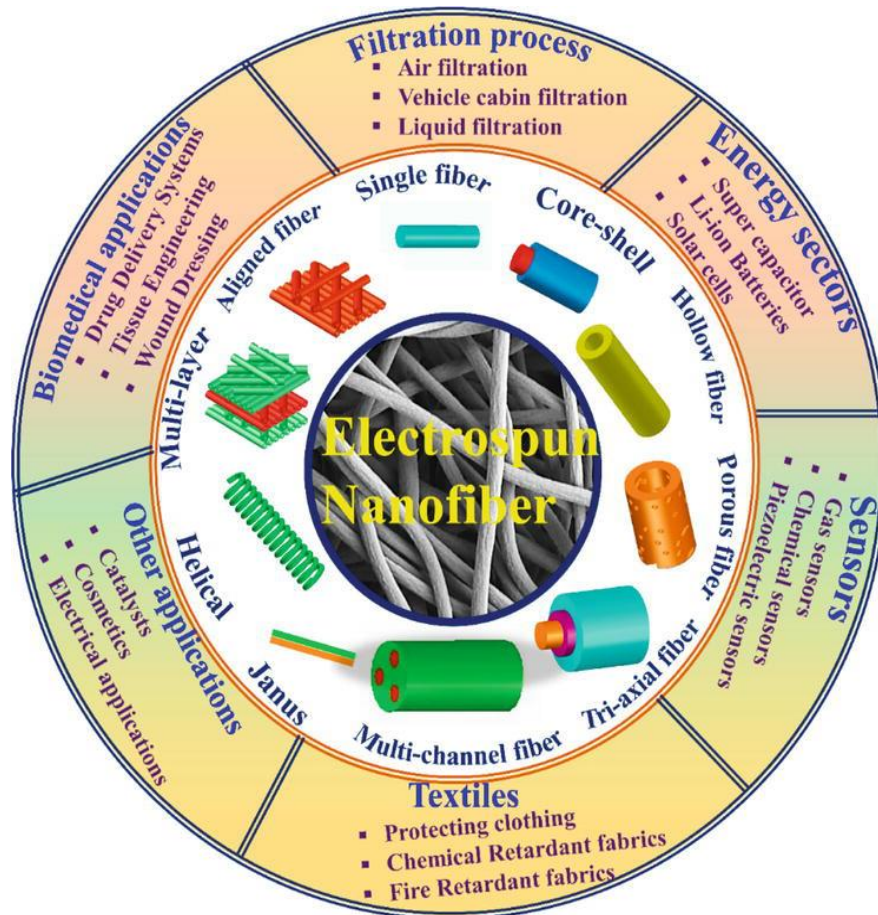


Figure 1.1: Areas of Application of Non-Woven Nano Fiber

1.4 Research Aim 1

Developing a scaffold using a feasible technique and materials to stimulate guided bone regeneration by supporting bone and improving bone regeneration capabilities.

The primary objective of this technique is to expedite the process of bone healing by and provide support to the site of bone fracture in order to facilitate guided bone regeneration. The intended approach involves utilizing high-performance polymers and biocompatible drugs to enhance the rate of bone healing and provide essential support to the bone during the development of an optimal polymeric scaffold. One

feasible technique for scaffold development is electrospinning. Electrospinning is a versatile and scalable technique that can produce nanofibrous scaffolds with high surface area and porosity, providing a suitable environment for cell adhesion, proliferation, and differentiation [10]. Electrospinning involves the application of an electric field to a polymer solution, which generates a jet of the solution that is stretched and solidified into nanofibers as it travels to a collector [11].

The electrospun scaffold's components need to replicate the extracellular matrix (ECM) of bone tissue. The ECM is a complex network of proteins and other molecules that provide structural support to cells and regulate their behavior. The most common materials used for bone regeneration scaffolds are synthetic polymers such as polycaprolactone (PCL), poly(lactic-co-glycolic acid) (PLGA), and polyethylene glycol (PEG), or natural polymers such as collagen, gelatin, and chitosan [12].

1.5 Research Aim 2

Analyze the scaffold structure and performance using chemical characterization, mechanical testing, and in vitro testing.

The purpose of these procedures is to gain a more complete assessment of the scaffold's properties, including its structural integrity, mechanical strength, and biological performance. This information is critical for determining the scaffold's suitability for use in various biomedical applications, such as tissue engineering (TE) and drug delivery [13].

Hydrophobicity and tensile strength are important development criteria because they provide enough strength to the scaffold to support the bone, which is crucial for guided bone regeneration [14].

Chemical characterization involves studying the scaffold's chemical composition to determine its properties, such as porosity, hydrophobicity, surface morphology, chemical bonding, and structure. Common techniques used in chemical characterization include Fourier transform infrared spectroscopy (FTIR), Transmission Electron Microscopy (TEM) and Scanning Electron Microscopy (SEM).

In vitro testing involves studying the scaffold's biological performance using cell culture experiments to evaluate its biocompatibility, cell adhesion, proliferation, and differentiation. Cytotoxicity tests are carried out to observe any changes in the cells' viability, morphology, or function in vitro tests that assess the ability of substances or materials to damage or kill living cells. These tests are often used in drug development, toxicology, and biomedical research.

1.6 Research Aim 3

Simulation based tensile analysis of scaffold. Simulate the scaffold to predict the effect of different compositions on tensile behavior of scaffold in future.

FEA-based tensile analysis can be used to predict the tensile behavior of scaffolds under different compositions, and this information can be used to optimize the scaffold's composition for specific applications [15].

Finite Element Analysis is a computational technique that can be used to simulate the behavior of complex structures under mechanical loading conditions. FEA can be evaluated using FEM. To predict the tensile behavior of a scaffold under different compositions, FEA can be used to model the scaffold as a 3D structure and apply a tensile load to it. The scaffold can be created using software such as solid works, and then imported into FEA software such as ABAQUS [15].

The first step in FEA-based tensile analysis is to define the material properties of the scaffold. In this case, the composition of the scaffold will play an important role in determining its mechanical properties. For example, the tensile behavior of a scaffold made from collagen will be different from one made from hydroxyapatite (HA).

FEA-based tensile analysis involves defining material properties, meshing the scaffold using finite elements, applying boundary conditions, solving equations of motion, and evaluating resulting stresses and strains to predict mechanical performance. Accuracy depends on factors such as mesh density, element type, and convergence criteria.

Chapter 2

Literature Review

2.1 Bone Structure and Function

2.1.1 Introduction:

Bone tissue is a considerably essential part of the body because it is the main structural part of the skeleton. It provides support for the tissues, protects critical organs, and serves as a fixation point for muscles that facilitate movement. The local function of bone in maintaining the skeletal system's integrity is of utmost importance. In the event of bone function loss due to injury, regaining it becomes necessary to preserve the skeletal consistency. Therefore, several clinical bone repair techniques have been developed to restore the lost bone function[16].

Bone has several functions in the human body, including as a reservoir for essential ions including calcium, zinc, magnesium, boron, titanium, and phosphate. These ions are essential for a variety of bodily processes, and their exchange between bone and extracellular fluid helps to regulate their concentration. Additionally, bone houses the hematopoietic marrow, which produces tissue-forming stem and progenitor, which develop into other cell types, and white blood cells that fight back infections. The understanding of functions is crucial for developing effective therapies for bone-related disorders[17, 18].

2.1.2 Classification of Bone:

Bones can be classified as long, short, or flat based on their shape. Long bones are cylindrical with expanded ends, short bones are cube-like, and flat bones have a thin, broad surface area. The structure and function of bones are better understood using this categorization[19].

All of the dimensions of short bones, such the tarsals and vertebral bodies, are about the same. The cranium bones are an example of a flat bone, which is shorter along one axis than the other. The femur and the tibia, the two longest human bones, are both cylindrical with broader ends.

Long bones are divided into three distinct sections depending on their proximity to

the "physis," also known as the growth plate. These regions are referred to as the diaphysis, metaphysis, and epiphysis, respectively. Bone development takes place at a specific site along each long bone known as the growth plate. [17].

Long bones in the body have three distinct regions based on their location relative to the growth plate, also called the physis. The central tubular area is known as the diaphysis, The metaphysis is the part of the bone connecting the diaphysis to the broadening ends. The epiphysis is the region at the end of longer bones outside the growth plate. The primary components of bone are shown in Figure 2.1 below[18].

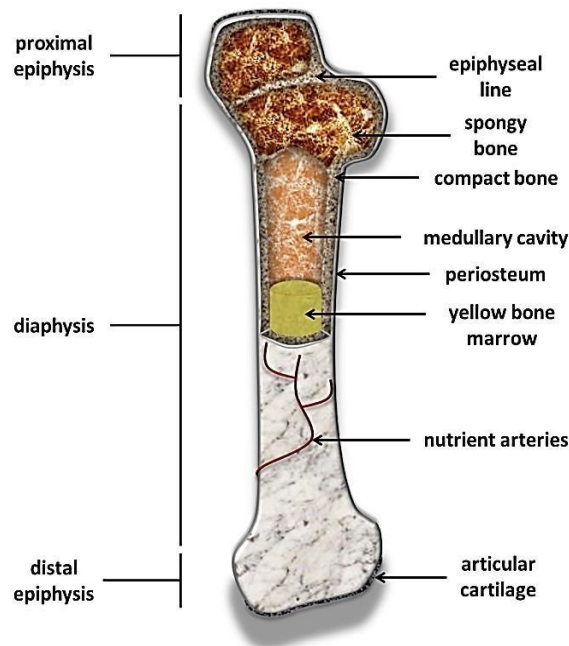


Figure 2.2: Primary Components of Bone

2.1.3 Cortical and Trabecular Bone:

Upon gross examination of bone cross-sections, the next level of hierarchy reveals a splitting of the skeleton into dense cortical bone and porous trabecular bone [20, 21].

Cortical/compact bone is characterized by a dense structure with minimal cavities, accounting for about 10% porosity. On the other hand, trabecular bone comprises porous areas with a vast network of interconnected cavities, making up 50-90% porosity[19, 22]. As a result of its unique architecture, cortical bone is highly able to withstand compression as compared to trabecular bone. However, trabecular network's high surface area allows it to absorb energy and deform more

effectively[23]. The trabecular bone is where most of the metabolic processes that keep bones healthy take place, whereas the cortical bone is there to support and protect the skeleton. What you see in picture 2.1 below is a representation of the relationship between trabecular and cortical bone[24].

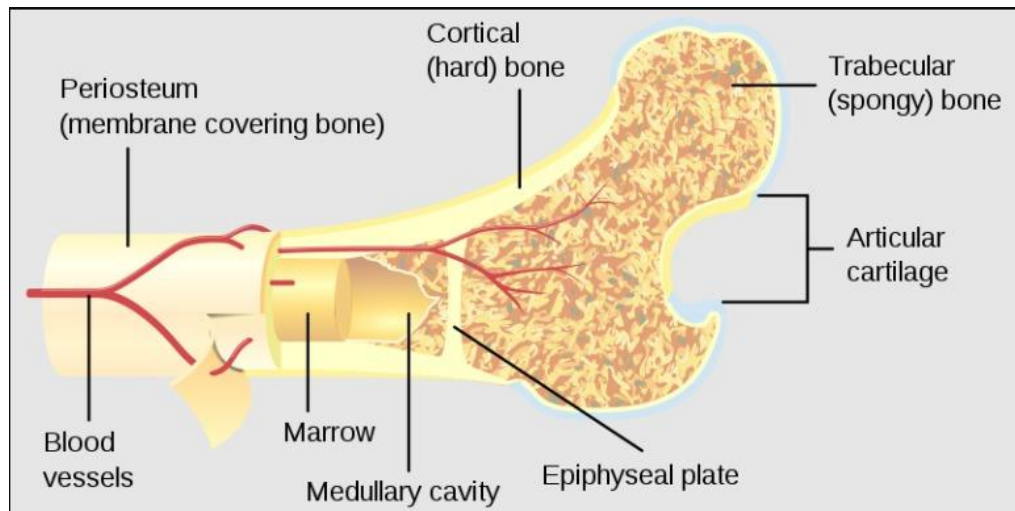


Figure 2.3: Relationship Between Trabecular And Cortical Bone

The microstructure and composition of the bone matrix are identical in cortical and trabecular bone. However, they differ in how the microstructure is arranged. Cortical bone has a repeating structure called the Haversian System or Osteon, composed of concentric lamellae. In contrast, trabecular bone has a porous structure consisting of plates and rods connected to each other. The epiphysis of long bones is predominantly consist of trabecular bone, with very thin layer of cortical bone covering the surface, whereas the diaphysis is predominantly made up of compact bone[25].

2.1.4 Bone Matrix:

Bone tissue is a unique kind of connective tissue that performs the duties such as structural support and protection. Bones are made up of cartilage and ossification tissue. The ultrastructure of bone tissue is made up of cells and extracellular matrix (ECM). Bone extracellular matrix (ECM) is a complex substance made up of both organic and inorganic components. The percentage of bone's dry weight contributed by its inorganic and organic components, respectively, is somewhere around 65% and 20%.respectively, while water accounts for the remaining weight [19]. The

inorganic portion of bone tissue comprises mineral crystals primarily composed of calcium and phosphorus, with lower levels of sodium and magnesium. The organic matrix also contains substantial amounts of amorphous calcium phosphate. Calcium and phosphorus-based hydroxyapatite ($\text{Ca}_{10}[\text{PO}_4]_6[\text{OH}]_2$) was once assumed to make up all of the mineral crystals. New evidence, however, suggests that the crystals also include acid phosphate groups and carbonate groups. [26, 27].

Bone tissue's organic component, which consists of cells and proteins, is predominantly collagen type I. Non-collagenous glycoproteins and bone-specific proteoglycans make up the remaining 10% and are considered to have a part in the bone matrix's structure and mineralization. Growth factors that affect bone cell activity include BMPs, IGF-1, and TGF- family members, are also present in the bone matrix. The organic matrix provides bone tissue with its tensile strength and structural integrity, while the inorganic matrix provides compressive strength. As a result of the mineral phase's connection with the fibers, bone tissue possesses a unique mix of hardness and toughness. The inorganic matrix stores ions and so contributes to the regulation of the body's internal environment (homeostasis).

2.1.5 Woven and Lamellar Bones:

Differentiating between woven and lamellar bone tissue is possible because of the bone matrix's structure. Primary bone, which includes woven bone, is relatively immature, whereas secondary bone, which includes lamellar bone, is fully developed [21]. Lamellar bone is distinguished from woven bone by its collagen bundles, which in the latter are organized in densely packed parallel sheets, generating lamellae that are generally 4-12 μm thick [19, 28]. Later in life, lamellar bone replaces the woven bone that was first created during growth and healing, making the woven bone less apparent. In addition, the number of cells in woven bone is much higher than that of lamellar bone. These bones have collagen lamellae which are either placed in a concentric pattern around a vascular canal or in a parallel arrangement. One may see the distinction between woven bone and lamellar bone in the following illustration [29].

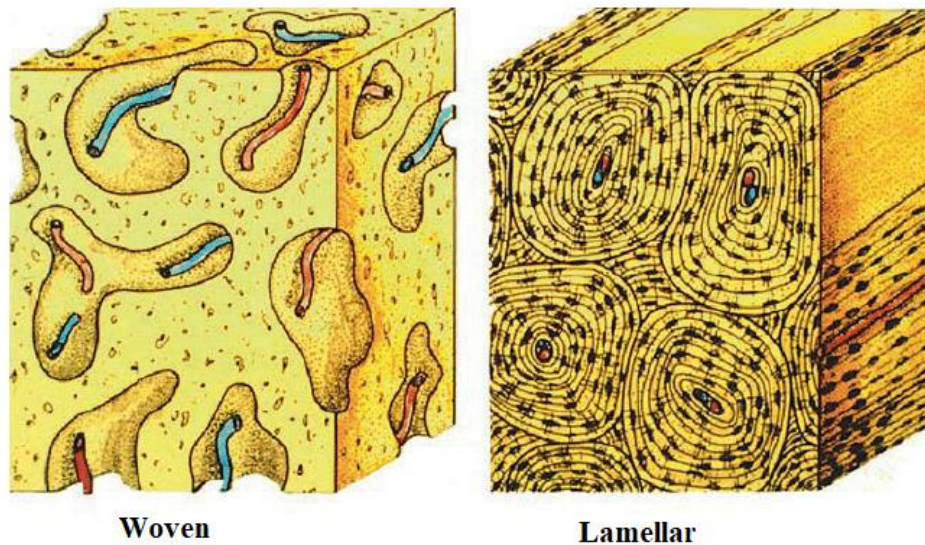


Figure 2.4: Woven Bone and Lamellar Bone

Bone tissue is organized into units called osteons, which are composed of stacked lamellae that encircle a central canal which holds nerves, vessels, and connective tissue. Woven bone is not stronger but more flexible than other lamellar ones because of its less structured matrix structure[21].

2.1.6 Bone Cells and Their Functions:

Many different kinds of cells are present in bone, which contributes to its extraordinary self-healing ability. Osteoblasts, osteocytes, and osteoclasts are the three major cell types found in bone tissue[19, 21]. The osteoblasts that make up bone cells are located on the outer layer of bone, in close contact to other osteoblasts. They are responsible for producing and secreting the organic bone matrix, as well as regulating its mineralization and remodeling. Osteoblasts exhibit significant alkaline phosphatase activity and adopt a cuboidal to columnar shape during matrix synthesis. They also have several Golgi membranes, endoplasmic reticulum, and mitochondria at this stage. Some osteoblasts become stuck in tissue while the matrix is produced around them, at which point they undergo differentiation into osteocytes. Some osteoblasts are retained on the bone surface but have limited functioning while others are somehow removed from the area [19].

Osteocytes tend to be critical to the process of maintaining and repairing the bone

matrix. Specifically, they reside in bony recesses called lacunae, which are surrounded by the skeleton's matrix. Osteocytes populate the spaces between and inside of the lamellae that make up lamellar bone. These cells contact neighboring cells via intercellular gaps and the canaliculi through which they stretch their long, branching cytoplasmic processes. These connections allow tiny molecules and ions to exchange. Not only do these connections facilitate the transport of nutrients and metabolites, but they also enable intercellular communication, which is essential for bone regeneration and repair.

Bone resorption and are two processes and rely heavily on osteoclasts, specialized cells. These cells are unlike monocytes in that they originate in the hematopoietic lineage yet share certain features with them. Osteoclasts, when activated, join the outer layer of bone, closing up the space between two. The osteoclast's membrane, which contacts the bone matrix, is highly folded in order to maximize the dissolution area and catch smaller particles. The bone minerals in the limited region dissolves in the acidic environment provided by proton transporters across the membrane.[30]. To digest the residual organic matrix, osteocytes release acid proteases. See Fig 2.2 for cell types and functions [31].

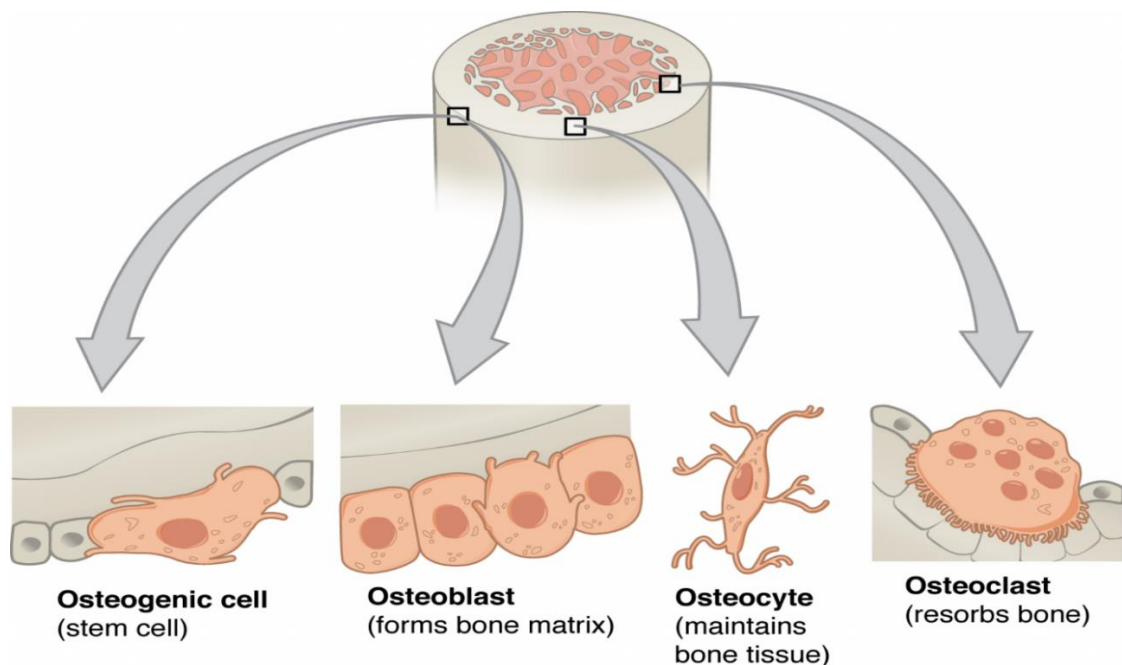


Figure 2.5: Cell Types and Functions

Among the three primary cell types, bone-lining cells have been discovered next to

the bone matrix [19]. They may help recruit osteoclasts and stimulate bone growth. Moreover, the periosteum, endosteum, blood vessels, bone marrow, and surrounding tissues all contain undifferentiated mesenchymal cells that have the potential to become osteoblasts[19, 32].

2.1.7 Periosteum and Endosteum:

Bones have a periosteum and an endosteum, which cover the outside and inside, respectively. Cells and connective tissue form a thin bilayer across these surfaces. Particularly important periosteum, which contains two layers of thick collagen fibrils and fibroblasts, as well as progenitor cells and blood arteries. By facilitating bone development and mending and supplying the bone with a substantial blood supply, it is vital to bone survival[33, 34]. The inner layer progenitor cells are responsible for callus development and remodeling during fracture healing, and periosteal cells can be used to generate bone tissue[35, 36]. Figure 2.3 provides a magnified view of the structure and position of the endosteum and periosteum layer[37].

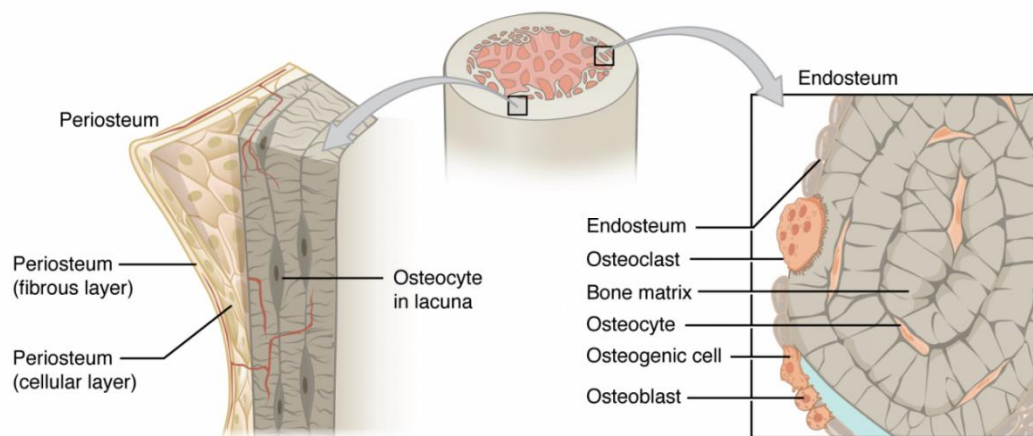


Figure 2.6: Structure And Position of The Endosteum And Periosteum

2.2 Bone Morphogenesis and Regeneration

2.2.1 Bone Development and Regeneration:

Bones form by either intramembranous ossification or endochondral ossification, both of which include the same process of matrix growth[38]. Cells called osteoblasts develop from mesenchymal cells and go on to produce bone. During mineralization, osteoblasts become osteocytes after being encased by the matrix. First, woven bone is

created, and later it is changed into lamellar bone. Bone creation is a two-step process, with osteoclasts removing old bone and osteoblasts depositing new bone. The intramural process of ossification starts with assembly of progenitor MSCs cells into layers at various sites.

As bone grows, multiple ossification sites form and merge to create a trabecular-like structure. These sites develop radially within the bone tissue and eventually form the entire bone. In intramembranous ossification, such as in the skull's frontal and parietal bones, bone tissue is formed directly from mesenchymal tissue without a cartilage intermediate.

While endochondral ossification takes place inside mesenchymal tissue, cartilaginous tissue is generated during endochondral ossification. Long bones, like femur and the tibia, are created by this method. Undifferentiated mesenchymal cells (UMCs) undergo a process of differentiation into specialized chondrocytes (C) that produce a cartilaginous matrix (CM) that ultimately assumes the structure of the bone to be generated. After the chondrocytes have grown, the cartilage matrix hardens, and they die. Once an osteogenic bud, made up of osteoprogenitor cells as well as vessels, penetrates cartilage, osteoprogenitor cells develop into osteoblasts, and creation of bone continues on the matrix of calcium-rich cartilage, which is left behind.

The health of the musculoskeletal system depends on bones that have the correct form and size. The formation of long bones from cartilaginous models is known as endochondral ossification.[21]. First, intramembranous ossification creates a bone collar in the perichondrium. Then, chondroclasts dissolve the calcified cartilage matrix as endochondral ossification continues. The diaphysis serves as the primary ossification center, and long bones have a hollow tubular structure due to bone growth longitudinally from this center and resorption at the center. The epiphysis has a secondary ossification center that expands radially, and the growth plate or epiphyseal cartilage separates the diaphysis from the epiphysis. As the diaphyseal bone replaces the epiphyseal cartilage, long bones grow longitudinally. Osteoblasts contribute to appositional growth of the bone collar, which causes long bones to grow in circumference.

2.2.2 Fracture Healing:

As compared to other adult tissues, bone has an extraordinary ability to mend itself. As bones recover, their biochemical and biomechanical qualities are fully restored, the formation of scar tissue is not a normal response to soft tissue injury. The process of bone fracture healing employs ossification pathways that closely resemble those seen in embryonic bone formation [39].

The healing of a bone fracture involves many stages, including initial inflammation, callus formation and strengthening, neovascularization, hemostasis, callus mineralization, and remodeling. [40, 41]. Hematoma, caused by bleeding from damaged blood vessels, is the initial stage of this process. Platelets released by the hematoma secrete vasoactive mediators and growth factors[17]. Following the initial acute inflammation, damaged tissues and cells are eliminated by macrophages. The lifeless ends of bones have no effect on the healing process. [42].

A callus tissue is first formed by periosteal cells and neighboring cells. This tissue wraps around the break and seals off the space between the two halves. The fracture callus is made up of osteoblasts, woven bone inside a membrane, and a mostly cartilaginous matrix. The callus reinforces the fragments of the fracture by connecting them. Calcified cartilage is penetrated by blood vessels along with osteoprogenitor cells. Like the development of the long bones in embryonic growth, this process involves removal of cartilage by chondroclasts and the deposition of immature woven bone by osteoblasts that have undergone differentiation. When callus is mostly made up of woven bone, tissue grows between the crack ends and remodels into lamellar bone, restoring the bone's natural form.

It's possible for both internal and environmental elements to affect how quickly a fractured bone heals. Growth factors, such as those in the BMP family, have shown promise in clinical studies as a therapy for promoting rebuilding after a crack. At the fracture site, these elements encourage new bone to develop[43].

Undifferentiated mesenchymal cells undergo a series of steps, including chemotaxis, mitosis, and osteogenic differentiation, in response to BMPs [44]. Additionally, there is a link between the growth of new blood vessels (angiogenesis) and bone growth[45, 46]. The healing process of a fracture is

significantly influenced by how it is stabilized[47, 48].

The typical way of healing a fracture involves endochondral ossification, which replaces the cartilage scaffold with bone. This process is commonly used for unstable fractures[48]. The reaction of the periosteum to a fracture is influenced by the level of motion in the affected area, with moderate motion enhancing the reaction and strict fixation minimizing it [42]. Additionally, intramembranous ossification may cure a fracture only if the bone ends are successfully rejoined. Additionally, it should be noted that increased activity at the site of the fracture can hinder vascularization and promote the formation of a cartilaginous callus[47, 49].

2.2.3 BMPs in Skelton Development and Fracture Healing:

A significant finding was made by "Marshal R. Urist" in 1965. Using demineralized rabbit extracellular matrix implanted in rat intramuscular pouches, he discovered that new bone may grow[50]. Urist later discovered the molecule in question and gave it the name bone morphogenetic protein. The genetic sequence of BMPs was later discovered in 1988, enabling their production through recombinant DNA technology[51].

The TGF-family of proteins includes bone morphogenetic proteins (BMPs), those are powerful agents that encourage bone growth. Around 15 types of BMPs have been found to date, and they are essential for the growth of the skeletal system, nervous system, and muscles [44, 52, 53]. In mice, BMP-2, -4, and -7 deficiencies can result in death during embryonic stages or shortly after birth, and BMP-2 deficiency has been linked to various abnormalities including those in the skull, hind limb, and kidney[54, 55]. BMPs 2, 4, and 7 are crucial for mending broken bones in adults[54, 56]. Certain bone regeneration therapeutics utilizing recombinant BMPs-2 and -7 have been granted FDA approval as of this writing.

When applied to MSCs and bone marrow-derived osteoprogenitor cells, BMPs generate a mineralizing phenotype. significant involvement in controlling cell activities by producing and differentiating into distinct cell types[44, 55, 57]. Lecanda et al. conducted a study showing that BMP-2 exposure to MSCs and osteoblasts resulted in increased mineralization of the matrix and higher amounts of proteins such as Osteocalcin, Osteopontin, and Bone Sialoprotein [58, 59].

Osteocalcin, a protein secreted by osteoblasts, contributes to bone strengthening, mineralization, and density. Additionally, as shown in Figure 2.4, Osteocalcin functions as a hormone, regulating insulin and blood glucose levels [60]. Moreover, BMPs guide MSCs towards specific chemicals to recruit the body's cells for tissue repair[61-63].

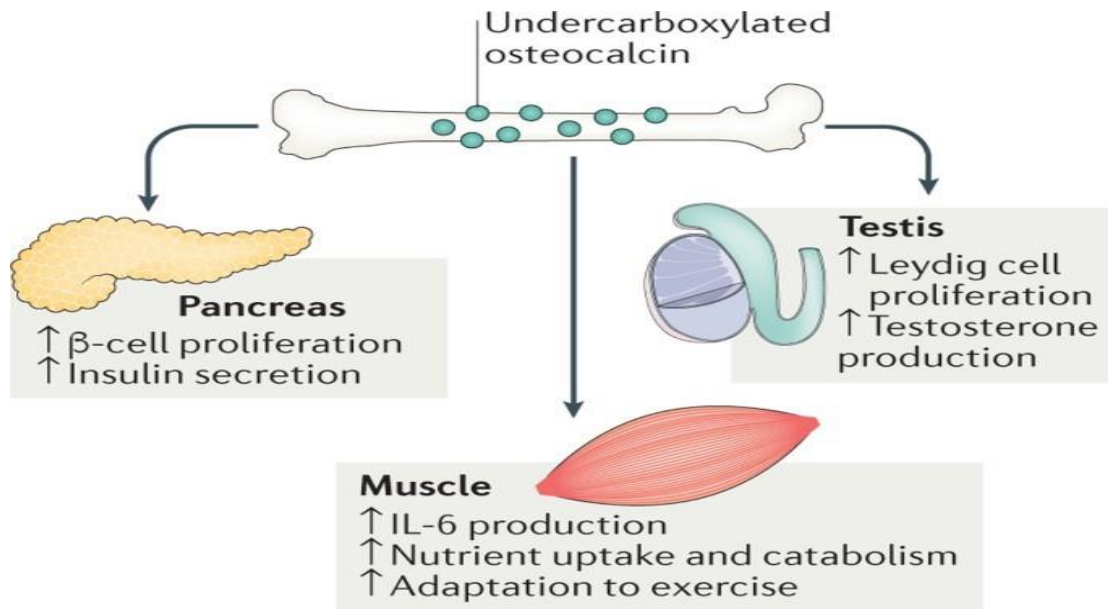


Figure 2.7: Osteocalcin Functions

Dimeric BMPs bind to receptors for serine/threonine kinases, activating intracellular effects. Signaling proteins called SMADs are activated when BMPs bind to their receptors; once within the nucleus, these proteins alter the production of transcription factors[57]. The inherent fracture healing response relies on BMPs to function properly. Bone breaks don't mend on their own in BMP-2 deficient mice[56]. When it comes to mending broken bones, each BMP performs an essential yet unique role[63]. Newly formed woven bone and an increase in MSCs that travel to fracture sites contain BMP-2, -4, and -7[64, 65]. To identify BMP-2 and BMP-4 sites and timing during fracture healing, Bostrom et al. employed a primary antibody that specifically recognizes these BMPs [64]. Bostrom et al. found that BMP levels were elevated in the periosteum's inner layer shortly following a fracture. Also, they noticed elevated BMP levels in osteoblasts and chondrogenitor cells around the mineralized cartilage matrix. In contrast, as the lamellar bone took the place of the woven bone, BMP expression decreased.

2.3 Bone Regeneration and Clinical Treatments

2.3.1 Clinical Needs for Bone Regeneration:

When bone is lost due to injury or illness, bone regeneration may be necessary to restore it. Joint arthrodesis, such as spinal fusion, requires the development of new bone tissue. Table 2.1 presents data on the number and success rates of bone augmentation treatments at a clinical site where joint

arthrodesis and fracture repair are the most common procedures. Although significant bone deformities and fracture nonunion are rare, this facility has been able to successfully treat these disorders. However, successful treatments often involve bone grafting techniques, which have several drawbacks. Nonunion and certain types of fractures are notoriously hard to treat, and they are increased by substantial bone abnormalities. High-risk fractures have a failure rate of up to 30% [43]. with open tibial fractures posing a significant challenge. Recent studies have shown that over half of patients receiving standard care for open tibial fractures experience treatment failure within a year of the injury Half of participants in another research had substantial disability seven years after surgery [66, 67].

Patients often experience joint pain and stiffness due to improper healing of bone fractures and defects, which can lead to disability [68]. In addition to physical symptoms, patients may also suffer from psychological distress following a traumatic event [69]. There is a significant monetary burden associated with bone disorders; in 2008, bone grafting procedures alone were projected to cost \$2.5 billion [70]. Furthermore, long-term rehabilitation and lost wages can exacerbate the burden on the healthcare **system**. Given the limitations of current treatments, there is an urgent need to proceed the cutting-edge technology in bone regeneration therapies.

The Cleveland Clinic's bone augmentation success rate and frequency. Data courtesy Dr. George Muschler.

Type	%	Success%
Nonunion	5	80-90
Cavity	10	~100
Fracture	20	95
Arthrodesis	60	80-90
Allograft Host Junctions	<1	95
Defects (>2 cm)	3	<50

Table 2.0-1: Bone Augmentation Success Rate and Frequency.

2.3.2 Clinical Bone Repair Strategies:

Conventional surgical procedures require the capacity to drill, cut, ream, and manipulate bone, which is contingent upon the skill of technicians and the quality of tools [19]. Although bone possesses remarkable regenerative properties, certain bone fractures and defects necessitate supplementary bone augmentation[68, 71, 72]. More than half million bone transplant operations done annually in the United States, with another 2.5 million performed globally[73, 74].

Bone grafting taken from the patient's own body, known as autologous bone grafting, has become the remedy of choice for bone regeneration since it supplies vital elements for bone repair[72]. Allograft bone has become more popular due to constraints such as morbidity at the donor site and a deficiency of graft material[75, 76]. While allograft bone provides an alternative, it has a higher rate of complications, such as late fractures and disease transmission, due to its reduced biological activity. Additionally, the inability of allografts to remodel often leads to failure[77, 78].

Newer bone graft replacements, such as ceramics and polymers, have been developed and are being widely used, but their limitations include fragility, lack of flexibility, little bioactivity, and low strength. As a result, there is growing interest in enhancing these materials with progenitor cells and growth factors to improve their performance[74]. New methods of promoting bone healing have been developed in response to the difficulties of conventional grafting techniques.

2.3.3 BMPs in clinical practice:

Since roughly twenty years ago, BMP(-2 and -7) (also known as rhBMP-2 and rhBMP-7) have already been exploited in the area of medicine. In addition to its usage in spinal therapies, rhBMP-2 applied to a type I collagen demonstrated to be effective in the management of open tibial injuries [79, 80]. Recombinant human bone morphogenetic protein-7 (rhBMP-7) and osteogenic protein-1 (OP-1) on a type I collagen carrier are also effective in treating tibial nonunion and facilitating spinal fusion, respectively [81, 82]. With a view to treating exposed tibial fractures, effectiveness of using rhBMP-2 in conjunction with nail fixing was evaluated in a clinical study that was randomized, controlled, and prospective. Nonunion rates were reduced by 29% and the need for further treatment was cut by 41% as compared to when just intramedullary nails were used. [79].

2.3.4 Drawbacks and Limitations of BMPs:

While BMPs have been experimentally shown to stimulate bone formation speed of broken bones, they need to be administered in very large quantities (3.5 to 12 mg), with a 1.5 mg/mL dosage superior to the gold standard. BMP distribution using collagen sponge has been shown to be ineffective, which necessitates the need for high doses and results in complications due to BMP diffusion. This high cost has led to BMP usage being reserved for last resorts.[83-85]. An extra £3.5 million is spent annually in the UK on BMPs for complex fractures, according to a cost-effectiveness study, with the price ratio depending on the cost of BMP and the complexity of the fracture.[86]. Thus, developing delivery devices to increase BMP distribution efficiency and reducing the amount of BMP used is crucial if this solution is to be cost-effective.

2.4 Research Approaches for Bone Regeneration:

2.4.1 Tissue Engineering/Regenerative Medicine (TE/RM):

it has evolved to include the creation of functional tissue constructs that can be implanted or used in vitro for drug screening and disease modeling. Tissue engineering of bone requires an addition of scaffolding, cells, and growth factors to generate a biocompatible tissue construct for implantation. The ideal scaffold would be a three-dimensional milieu similar to the original extracellular matrix, which would then facilitate cell attachment, proliferation, and division while also degrading in a regulated manner as new tissue develops. Many cell types have been employed in bone tissue creation. They include MSCs, osteoclasts, osteoblasts, and chondrocytes. Cell proliferation, division, and angiogenesis can all be boosted by administering growth factors including BMPs, as well as the growth of vascular endothelial factor.[16, 87]. The potential for improved and less expensive bone regeneration techniques is promising thanks to the domain of BTE.

In the laboratory, cells are cultured on scaffolds to produce tissue substitutes that can be transplanted into living organisms at a later time. For thin tissues with poor regeneration potential and restricted vascularity, such as cartilage, the "in vitro tissue engineering" method has proven successful in producing skin replacements [88-91]. But still, without a blood supply, mass transfer is limited, making it difficult to generate and sustain massive vascularized tissues like bone.[92].

In order to promote repair mechanisms with minimal in vitro manipulation, certain strategies have proven effective for tissues with high regeneration capacity, such as bone [93-95]. The objective of these procedures is to activate the patient's natural repair mechanisms by delivering growth factors directly to the injured site. Tissue engineering performed in vivo might speed up the approval and commercialization processes because it doesn't need as much time in a lab. The term TE/RM now encompasses all techniques used to substitute, repair, or regenerate damaged tissues or organs, regardless of whether they are performed both in vitro and in vivo [96]. Earlier, regenerative medicine was often associated with stem cell technology, but it has now been integrated into tissue engineering to form the TE/RM field [16, 87, 97, 98]. Biological components, such as scaffolds, stem cells, proteins, peptides, genes, and

more, are all included in the range of TE/RM techniques for bone healing [98-104].

2.4.2 Scaffolds:

Scaffolds are important in tissue regeneration and regeneration because they serve as a foundation upon which new tissue can develop. Scaffolds were once only used for structural support, but recent developments in biomaterials have allowed for the creation of functional scaffolds that may also affect cellular response[105, 106]. Scaffolds with varied chemical and physical characteristics are the result of a number of fabrication methods. In rapid prototyping, a three-dimensional structure is built by depositing layers of material in exact layers. Salt leaching involves the use of salt particles to create pores within the scaffold. Phase separation uses a mixture of polymers that phase-separate into two distinct phases, creating a porous scaffold. Gas foaming utilizes the expansion of gas bubbles to create a porous structure within the scaffold [16, 107-111]. Scaffolds with a large hole size and interconnected porosity, which promote the formation of blood vessels as well as cells, are often used in the field of BTE. Biocompatible and able to promote bone formation, ceramics like hydroxyapatite (HA) and calcium phosphates (TCP) find widespread application. Because to their biodegradability and adjustable mechanical characteristics, synthetic polymers like poly(-caprolactone) (PCL) and poly(lactide-co-glycolide) (PLGA) are also employed[95, 108, 112].

While structural scaffolds have been used for bone growth, they can have limitations due to slow resorption kinetics and a poor cellular environment. To address these limitations, researchers have explored infusing scaffolds with growth factors like rhBMP-2 [95]. While rhBMP-2-infused PLDL scaffolds stimulated bone ingrowth, the study discovered that they were unable to heal long bone defects due to their delayed material degradation. This led to limited bone growth within the scaffold after 16 weeks[95]. To promote bone repair using a different approach, the technique of guided bone regeneration (GBR) involves the placement of two-dimensional membranes along the periosteal surface to encourage bone growth. This differs from the use of 3-D structural scaffolds typically employed for bone growth[113-116].

Guided bone regeneration (GBR) utilizes two-dimensional membranes placed along the periosteal surface to encourage bone repair, unlike the 3-D structural scaffolds used for this purpose. When placed on the defect's edge, these membranes allow tissue to deposit

into the open region, potentially resulting in the full repair of the defect. Electrospun non-woven nanofibers are a novel form of membrane with the potential to improve GBR by increasing cell adhesion and function by mimicking the shape of the extracellular matrix [117-119]. Hydrogels, which have a gel-like structure, are another interesting type of scaffold. While their mechanical qualities may be inferior, they allow cell migration and remodeling and can be injected using minimally invasive surgical techniques, making them advantageous for bone tissue repair. Additionally, these materials can be used not only as scaffolds, but also as carriers for biological components to the site of injury.[120, 121].

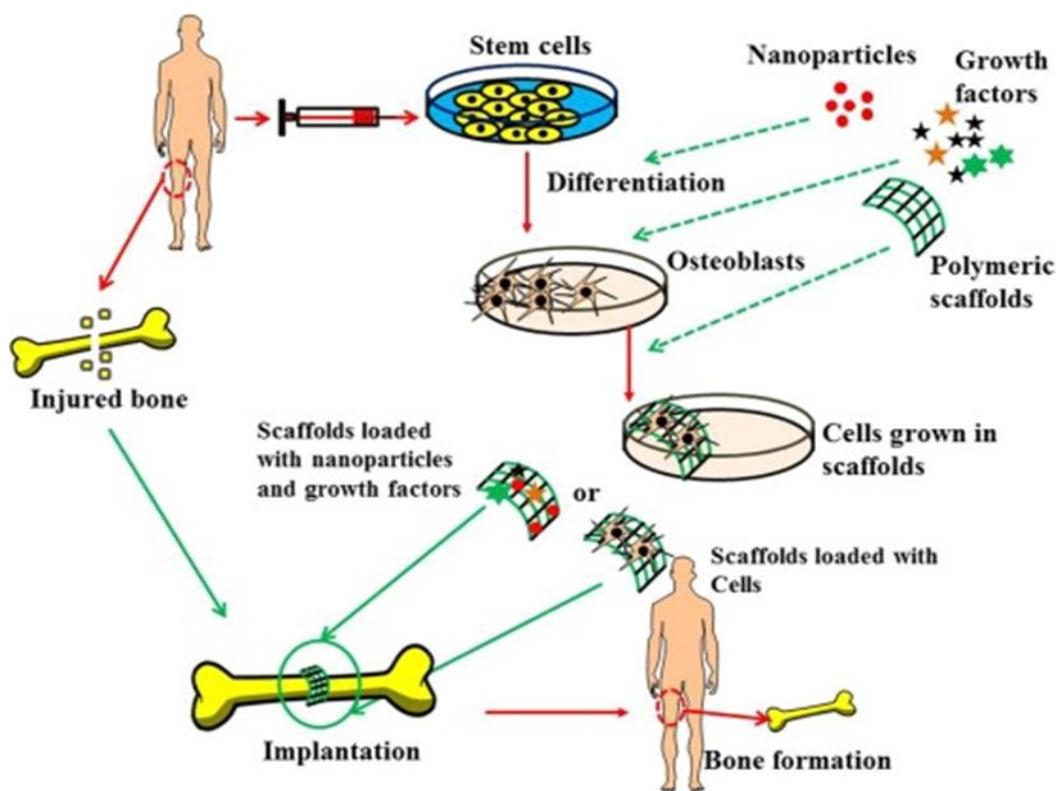


Figure 2.8: Biological components to the site of injury

2.4.3 Cell Sourcing and Delivery:

While acellular techniques using scaffolds and BMPs have shown clinical effectiveness in bone repair, some individuals with reduced osteoprogenitor cells may require osteogenic cell therapy for optimal bone regeneration. Those over the age of 65, those with severe wounds or metabolic abnormalities, smokers, and those undergoing chemotherapy or radiation are all examples [122]. In order to be successful, cell-based therapies need to locate a cell source that is not only

accessible, but also can be cultivated in high quantities and possesses bone regeneration potential [123, 124]. In the field of BTE, MSCs isolated from bone marrow have been investigated extensively because of their ability to speed up the repair of major bone lesions in animal trials. [125-127].

MSCs harvested from bone marrow have a limited ability to self-renew, and this capacity declines with the age of the donor [128, 129] Additionally, the differentiation potential of MSCs can also be affected by age, with decreased osteogenic potential observed in older individuals[130, 131].

Recent research has revealed pluripotent Cell types with c-Kit expression in the amniotic fluid of humans and rats[132]. Both human and amniotic fluid or the amnion membrane been demonstrated to include pluripotent cells expressing c-Kit. Amniotic fluid stem (AFS) cells have been found to be capable of differentiating inside cells of the embryo's three separate germ deposits. They are a potential resource of regenerative cells since they can develop swiftly without feeder cells, and they do not generate tumors. AFS cells effectively divided into the bone-forming and cartilage-forming lineages of chondrogenesis [133, 134].

When developing tissue-engineered structures in vitro, a common problem is that the cells and tissue tend to grow only on the outer edge, leaving a hollow core due to limited nutrient delivery [135-138]. Similarly, when there is no early blood supply in damaged bone, the core of the defect may not receive adequate minerals and nutrients. The survival of the core cells is often affected when cells are transplanted at the damage site in vivo on a three-dimensional scaffold.[139, 140]. Instead, cells can be implanted into a tissue-engineered periosteum that will surround the defect and provide blood supply, which may increase cell survival.

Because of the enhanced transport environment, the cells may move to the Centre after a consistent vascular network has been created there. BMP-2 producing BMSCs implanted through Allografts covered in gelfoam. have been proven in recent studies to increase graft integration and healing[141].The unique structural features of Electrospun nanofibers enhance cellular adhesion and proliferation, making them a potential material for bone implantation.

Chapter 3

Overview of Developed Method and Models

In this chapter, the general overview of the fabrication, and simulation method developed are discussed here.

3.1 Electrospinning:

Electrospinning is advantageous because it can manufacture nanofibers with a variety of topologies (monolithic and coaxial) at a high pace and with little effort.

Cooley and Morton created "Electro Spraying" in 1902 for low molecular weight and low viscosity fluids; The fundamental contrast between "Electro Spraying" by Cooley and Morton and "Electrospinning" by Formhals is the fluid viscosity. With the invention of Formhals, electrospinning has been widely used in materials science and nanotechnology to manufacture nanofibers with unique properties applications[142, 143].

Formhals introduced electrospinning in 1934 for higher viscosity solutions, such as polymers. When spinning cellulose acetate fibers in an acetone/alcohol solution, Formhals aligned the fibers using a roller-like equipment. That was the first-time nanoscale fibers could be spun successfully using electrospinning technology, and it represented a tremendous advancement [1]

Formhals' idea improved electrospinning, but it also had drawbacks. Due to the inability of the solvent to evaporate from the fiber jet before it reached the collector, the supercharged polymer solution created a disorganized web. It was challenging to extract the fibers because they stuck to the collector, to one another, and to the solvent, which had not yet evaporated. With his second invention, Formhals extended the distance between the spinning and collecting places in order to address a number of flaws in his original design[144].

The second innovation of Formhals is a method for spinning multiple fibers from a single polymer solution by directing fiber streams to a collector using a number of nozzles. In 1940, Formhals invented a technique for creating composite fibers by electrospinning a polymer solution onto a rotating foundation line[145].

The researchers subsequently shifted their focus to electrospinning, although it would be almost 30 years before Taylor published his discoveries on the jet manufacturing method. Taylor explored the effect of an electric field on a polymer droplet at the tip of a capillary in 1969. Taylor mathematically duplicated electrospinning to show the impact of electric force on fluid droplets, resulting in a cone-like shape that is now commonly known as a "Taylor cone." [146].

Baumgarten began researching the influence of solution and processing variables on the structural properties of electrospun fibers in 1971. After a PAN/DMF solution was expelled from a metal capillary, he inspected the solitary fiber missing from the electrified polymer. When he discovered that the diameter of the fibers increased according to the viscosity of the fluid, he realized the procedure was effective[147, 148].

Following BAUMGARTEN's groundbreaking research, it is now possible to alter the structural features of electrospun fiber by the electrospinning of polymer melts. LARRONDO and MANDLEY produced electrospun fibers by melting polyethylene and polypropylene[149, 150].

During the same time period, tissue engineers were also developing Electrospun fibers. In 1978, ANNIS and BORNAT examined the use of electrospun polyurethane mats as a potential vascular prosthesis[151]. In 1985, FISHER and ANNIS initiated research on the in vivo endurance of electrospun vascular prosthesis[152].

Although these early attempts to utilize electrospun fiber sheets in tissue engineering and drug delivery applications, it would take more than a decade for electrospinning to become widely adopted as a polymer processing technique, researchers have made significant strides in their knowledge of the nano- and microscale applications of these nanofibers, which contributed to the development of electrospinning in the 1990s [153-155]. In the twenty years following the discovery of electrospun nanofibers, Electrospinning has become a versatile approach for generating nanoscale

2D and 3D scaffolds as a consequence of increasing research in both academic and industry contexts[156-159].

3.1.1 Electrospinning Working Principle:

A metal roller collector, a high-voltage source of power, and a spinneret portion are the three main parts of an electrospinning machine[160, 161].

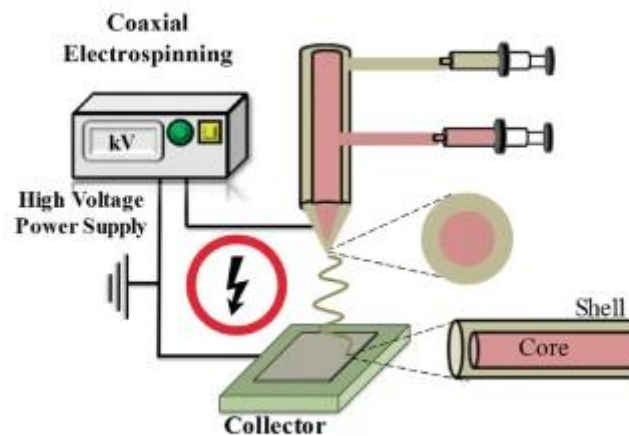


Figure 3.9: Scheme of Electrospinning Working

The spinneret portion includes a polymer solution storage chamber, an injector with a very fine metal needle (the spinneret), and an injection actuator. Here, the drug/polymer solution is distributed at an even rate[162]. The precursor droplet is charged by either DC/AC applied to the needle's tip. By linking the tip of the coaxial needle to an external voltage source, this generates a coulombic force that pulls on the needle [163, 164]. Tension on the surface, electrostatic and viscoelastic effect, gravitational force, and air drag are some of the forces that are working together at the same time.

In the process of electrospinning, polymeric nanofibers are formed from a liquid jet using the previously discussed forces. The manufacturing of nanofibers consists of three main steps: This process has three phases:

- 1) Formation of a straight-line jet, which begins at the needle's tip.
- 2) Bending deformation accompanied by looping and swirling trajectories.
- 3) Solvent evaporation results in the formation of solid nanofibers[165].

3.1.2 Process Parameters:

Electro spinnability refers to the ability of a viscoelastic liquid to initiate jets and spin continuously under an applied electric field, resulting in continuous fiber production with constant fiber diameters and few bead-on-string imperfections[166]

Multiple lab studies have been carried out to study the three primary factors related to electrospinning materials as well as process parameters.

- **Solution Properties:** viscosity/concentration, conductivity, molecular mass, tension on surface, and solvent properties.
- **Process Parameters:** needle-to-collector distance, flow rate of solution, and voltage.
- **Ambient Conditions:** humidity level and temperature

All of these factors have an impact on the procedure and are crucial when selecting the final product's quality when it comes to electrospun nonwoven fibers [167].

The viscosity of the polymer solution, which is related to the solution's concentration and tension on its surface, is one of the most important elements in determining the nanofibrous structure's overall form[168]. Multiple studies showed that higher viscosity polymer solutions resulted in fibers with greater length[169-171].

3.1.2.1 Solution Viscosity/Concentration:

The solution's spinnability depends on the polymer concentration; the polymer concentration must be high enough for chain attachments to develop without being overly dilute or too viscous[172] therefore, electrospinning works best at a certain degree of viscosity that is unique to each kind of polymer.

3.1.2.2 Conductivity:

Because of the increased tensile stress experienced by the fiber jet during electrospinning, the nanofiber diameter is significantly reduced when the solution has a high conductivity. Additionally, the electrospun nanofibers may benefit from increased elongation forces provided by ions with lower radii due to their higher charge density[173].

3.1.2.3 Molecular Weight:

Electrospun fibers' structure is significantly impacted by the polymers' molecular weights. The viscosity of a solution is an accurate indicator of its molecular weight because it measures the degree to which polymer chains interact in the solution[174]. Beads, rather than continuous fibers, would develop in a solution of a low-molecular-weight polymer at a constant concentration. Even at low concentrations, high-molecular-weight polymers may promote micro ribbon production[174, 175].

3.1.2.4 Surface Tension:

The molecular weights of the polymers have a profound effect on the structure of electrospun fibers. Because it measures the degree to which polymer chains interact in the solution, a solution's viscosity is an accurate indicator of its molecular weight. In a constant concentration solution of a low-molecular-weight polymer, beads would form rather than continuous fibers. High-molecular-weight polymers can promote micro ribbon production even at low concentrations[176].

3.1.2.5 Solvent Selection:

When electrospinning a certain polymer into nanofibers, the solvent of choice is crucial. When selecting a solvent, it is important to consider both the polymer's solubility and solvent's boiling point. The nanofibers' dehydration during their path from the needle tip to point of collecting surface is aided by volatile solvents, making them the preferred option. Because of their low boiling temperatures, they also evaporate quickly.

However, low-boiling-point solvents should be avoided since their evaporation at the capillary tip may block the tip and reduce the rate of flow of solution. Nanofibers with a ribbon-like, flat structure or clotting of nanofibers at the borders may form if a

solvent with a high boiling point does not dehydrate completely before reaching the collector.[172, 177, 178].

3.1.2.6 Voltage:

Since the amount of charges supplied to the solution is mostly determined by the operating voltage, the latter plays a crucial role in electrospinning[179].

While greater voltage may cause the solution droplet to expand, resulting in a longer jet, shorter flight times may reduce the jet's ability to stretch before deposition. As a consequence, the fiber starts off narrowly, but as the voltage increases, the diameter begins to decrease. A smaller fiber diameter is achieved by continuously raising the voltage, which speeds up the electrospinning flow and draws more solution out of the needle's tip. Research shows that increasing the voltage supplied will cause the solution to be stretched farther, leading to fibers that are less thick[180, 181].

According to research conducted by Wu et al., fiber diameters decreased as voltage increased up to a critical point, after which the behavior reversed[182].

3.1.2.7 Tip-To-Collector Distance:

The distance from the jet's point to the collector determines the stage of instability at which the spray lands on the collector, with a sufficient distance allowing for ample travel time and solidification. As the distance between the tip and collector increases, the diameter of the fiber could decrease. However, the significantly diminished field intensity beyond a given distance may result in an increase in fiber diameter[183, 184].

3.1.2.8 Flow Rate:

Typically, the diameter of electrospun nanofibers is unaffected by the flow rate; however, this factor must be adjusted in order for the solution to be distributed and taken off the nozzle tip [185, 186].

When the flow rate exceeds enough, an increase in filament diameter and the presence of beaded fibers can be observed due to the larger size and initial radius of the spinning jet, as well as the decreased stretching forces and shortened drying time before reaching the collector[187-189].Development and diameter of nanofibers are

influenced by the flow rate, and a minimal flow rate is preferable in order to feed the solution constantly throughout jet development[190].

3.1.2.9 Humidity:

Polymer elongation ceases if moisture condenses on the outer layer of any electrospinning jet, particularly in humid environments where the polymer precipitates quickly[191]. In contrast, it has been shown that at higher relative humidity, quicker solvent vaporization reduces fiber diameter, with the resulting diminution in fiber diameter being predominantly ascribed to a commensurate diminution in the precipitation effect[192, 193]. When using a dual solvent approach, humidity is also shown to have a substantial effect on the production of porous nanofibers.

3.1.2.10 Temperature:

Thinner fibers result at higher temperatures because the solvent evaporates more quickly, and the polymer solution has less viscosity[194].

3.1.2.11 Fiber Alignment:

The initial metallic plate collector is covered with nanofibers that have been randomly orientated during fabrication. The arrangement and configuration of electro spun nanofibers may be affected by design choices made for the collector. Different collector systems, including those constructed of metallic and dielectric materials, have been designed in an attempt to enhance the alignment of electro spun fibers. There are a few of the methods that have been tried in an effort to achieve alignment in electro spun nanofibers[195].

In order to obtain a circumferential orientation of electro spun nanofibers, it has been suggested that a cylinder collector be rotated at up to a thousand revolutions per minute[118].

The fibers are picked up on the outer layer of the cylinder firmly in a circumferential way, leading to a fair alignment, when the longitudinal speed of the revolving cylinder surface, which acts as a fiber adoption device, equals that of evaporated spray depositions. The term for this velocity is alignment velocity. Since the final

deposition way is determined by the quick chaotic movements of jets, collecting randomly produced fibers will occur if the outside velocity of the cylinder is less than the alignment speed. However, the take-up speed cannot be too high, or the fiber jet would be broken, and hence there has to be a maximum rotation speed at which no new fibers can be gathered. While the revolving wire drum collector can collect precisely oriented fibers, producing a larger layer of oriented fibers is challenging due to residual charge buildup on the collected fibers, which disturbs the proper positioning of new fibers[196].

Bhattarai et al. described a rotating cylinder encircled by a wire that could produce fibers with a high degree of alignment. Aligned fibers were focused on the wire rather than the full drum, and their collection area on the wire could be adjusted by changing the wire's thickness[197].

3.2 Freeze Drying:

Freeze-drying, also known as lyophilization, is a process that is commonly used in scaffold fabrication for tissue engineering. by using this technique scaffolds with 90% porosity and pore size ranging from 20-400 μ m can be obtained[198].

Freeze-drying is particularly useful for creating scaffolds from materials that are sensitive to high temperatures or chemicals, as the process is gentle and does not involve harsh chemicals.

It involves removing water from a material by sublimation, which is the direct transition of a substance from a solid state to a gas state without going through a liquid state.

In scaffold fabrication, freeze-drying is used to create porous structures that mimic the natural extracellular matrix (ECM) of tissues. The scaffold material is first frozen, and then placed under a vacuum, causing the water within the scaffold to sublime. This leaves behind a porous

structure with interconnected channels, which can be used to support cell growth and tissue formation. The utilization of hydrophobic vessels promotes the removal of aqueous solvents, thereby enhancing the efficiency of the procedure[199].

Additionally, the resulting scaffolds have a high porosity, which can promote nutrient and oxygen diffusion, facilitate cell infiltration, and improve overall tissue regeneration.

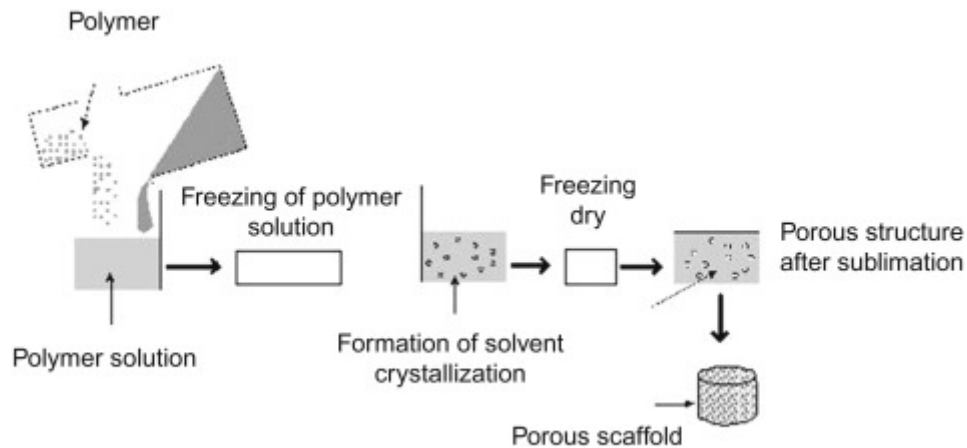


Figure 3.10: Freeze Drying Process

3.2.1 Drawbacks and Limitations of Freeze Drying:

While freeze-drying is a valuable process for scaffold fabrication, it also has some drawbacks and limitations that should be considered. Here are a few:

- a) **Cost:** Freeze-drying is an expensive process, requiring specialized equipment and expertise. This can make it prohibitively expensive for some applications.
- b) **Time-Consuming:** Freeze-drying can be a slow process, especially for large scaffolds or materials with high water content. This can lead to longer manufacturing times and potential delays in research or clinical applications.
- c) **Brittleness:** The freeze-drying process can lead to a brittle scaffold structure, which can affect its mechanical properties and limit its usefulness for certain applications.
- d) **Limited Scalability:** The production of freeze-dried scaffolds can be difficult to scale up for large-scale manufacturing. This can limit the availability of freeze-dried scaffolds for clinical applications.

- e) **Risk Of Contamination:** The freeze-drying process can increase the risk of contamination if the equipment or materials are not properly sterilized. This can be a significant concern in clinical applications.
- f) **Limited Control Over Pore Size and Distribution:** The pore size and distribution in freeze-dried scaffolds can be difficult to control, which can limit their effectiveness for certain tissue engineering applications.

Overall, while freeze-drying is a valuable process for scaffold fabrication, it has some limitations that should be considered when choosing a fabrication method.

3.3 Bio-printing:

Bioprinting is a process that uses 3D printing technology to create complex 3D structures that contain living cells. In scaffold fabrication, bioprinting is used to create scaffolds that mimic the natural extracellular matrix (ECM) of tissues and organs.

The bioprinting process involves the use of a printer that is capable of depositing living cells, biomaterials, Ceramic-based materials like HA, ECM-derived materials include such as laminin and fibronectin. or a combination of all, layer by layer, in a predetermined pattern.[200]

The 3D digital models created using computer-aided design (CAD) software are what make bioprinting so special; they allow for the creation of layered, complicated, and adaptable geometries. The printer head moves back and forth across the scaffold, depositing the biomaterials and cells in a precise manner, according to a digital design [201].

3.3.1 Bio-Printing Process:

The bio-printing process generally involves the following steps:

3.3.1.1 PRE-PRINTING:

This step involves designing a 3D model of the tissue or organ that needs to be printed using computer-aided design (CAD) software. The 3D model is then sliced into thin layers [202] and the necessary parameters, such as the type of bio-ink, the printing speed, and the temperature, are determined.

3.3.1.2 Bioprinting:

During this step, the bio-ink is loaded into the printer and the printing process begins. The printer precisely deposits layers of bio-ink, following the design created in the pre-processing/printing stage, and builds up the 3D structure layer by layer[203].

3.3.1.3 Post-Printing:

Once the printing process is complete, the printed structure undergoes post-printing. This step involves removing any support structures that were used during printing, and then curing the printed tissue or organ using techniques such as UV light exposure, maturation in bioreactor or chemical cross-linking [204]. Finally, the printed structure is evaluated for quality, and any necessary modifications or improvements are made.

The bioprinted scaffold can then be placed in a culture environment, where the cells can grow and differentiate, forming functional tissue[205] Bioprinting allows for the creation of complex, multi-layered structures with a high degree of precision, which makes it an attractive option for tissue engineering. **FIGURE** shows three steps of bioprinting process[206].

Bioprinting has been used to produce a range of tissues and organs, including skin, cartilage, bone, liver, kidney, heart, and blood vessels.[207-211].

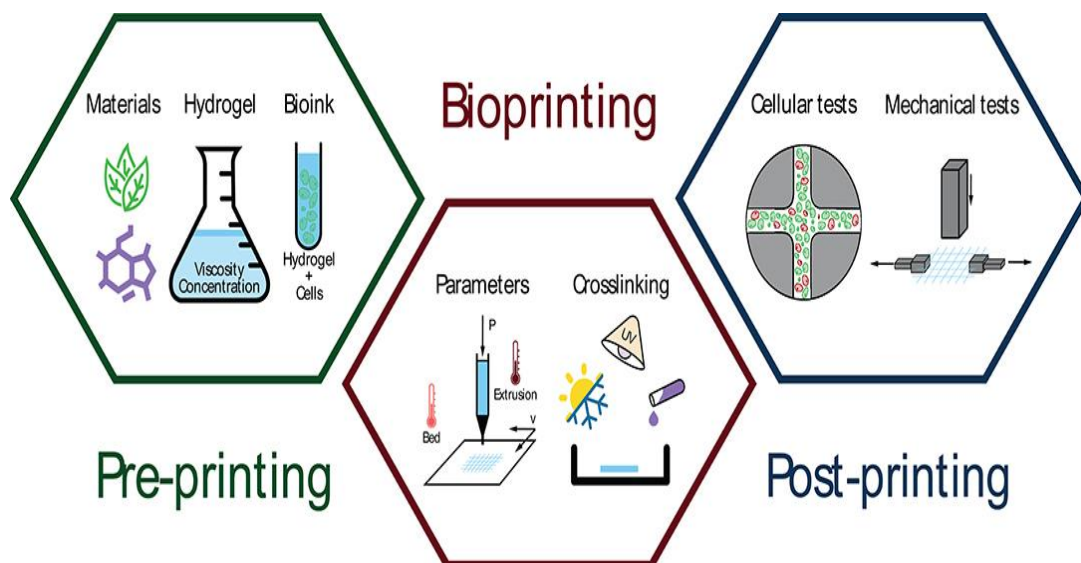


Figure 3.11: Bio Printing Process

3.3.2 Parametric Considerations:

3.3.2.1 Position of The Print Head:

The print head is responsible for depositing material, layer by layer, to build up the final 3D object. If the print head is not accurately positioned, the layers may not align correctly, leading to a distorted or imperfect final product.

The bio assembly tool (BAT) is typically controlled by computer-aided design/manufacturing (CAD/CAM) software that generates the 3D model of the desired tissue or organ structure. The software then converts the digital model into instructions that the BAT can follow to deposit the cells layer-by-layer in a precise and controlled manner[212].

By moving the printing heads in the X and Y directions and controlling the height of the printing platform, the BAT can deposit cells and biomaterials at precise locations and with precise thicknesses[213].

3.3.2.2 Development of Bio-Ink:

Bio-ink is a key component of the bioprinting process and remains a challenge while selecting and developing bio-ink because they serve as a carrier for cells and other biomaterials, allowing them to be deposited in a controlled and precise manner.

The ideal bio-ink should be biocompatible, biodegradable, and capable of supporting the growth and differentiation of cells. It should also have suitable mechanical and rheological properties to enable the printing of complex tissue structures with high reliability. In addition to biomaterial selection, other factors such as cell density, viscosity, and crosslinking also play a critical role in the development of bio-inks[214].

3.3.2.3 Bio Printer Head Type Selection:

Bio printers are divided into 3 types of Extrusion-based bio printers, Inkjet-based bio printers and Laser-based bio printers.

- a) **Extrusion-Based Bio Printers:** This type of bio printer uses a syringe or nozzle to extrude a bioink, which is a mixture of living cells and a supporting material. The bioink is deposited layer by layer to create the desired biological structure. This technique is feasible for solutions with different viscosities and offers better structure properties along with high printing time[215].
- b) **Inkjet-Based Bio Printers:** Inkjet-based bio printers use a printhead to deposit droplets of bioink onto a substrate. The droplets can be deposited in precise locations to create complex biological structures. Inkjet technique is low cost and suitable and keeps low chances of contamination. The lifespan of cells may be negatively impacted by factors such as high temperature and vibration. The occurrence of needle blockage may lead to processing difficulties[216].
- c) **Laser-Based Bio Printers:** Laser-based bio printers use a laser to create patterns on a substrate, which are then populated with living cells.[217] This technique is suitable for high viscosity inks like hydrogels. Typically, the production rate is low and laser produces excessive heat that is a potential risk for damaging cells[215].

In 3D bioprinting, the technology and selection of print head used for the process play a critical role in determining the success of the experiment. Several factors need to be taken into consideration to ensure that the chosen technology and print head are suitable for the specific application.

One of the key factors to consider is the characteristics of the cells being used. Different cell types have different requirements for growth and differentiation, and the technology and print head should be chosen based on the cell type and its characteristics.

3.3.3 Advantages of Bio Printing:

There are several advantages to using bioprinting for scaffold fabrication. For example, bioprinting allows for the precise placement of cells within the scaffold, which can improve cell viability and promote tissue formation. Additionally, bioprinting can be used to create scaffolds with specific mechanical and chemical properties, which can be tailored to meet the needs of different tissue types[218].

3.3.4 Drawbacks & Limitations of Bio-Printing:

However, there are also some limitations to bioprinting that should be considered. Materials used for bioprinting can be limited in terms of their availability and biocompatibility[219].the bioprinting process can be time-consuming and expensive therefore bio printing is only feasible for small scaffolds, and the Additionally, the long-term stability and functionality of bioprinted scaffolds are still being studied and understood, and regulatory approval for clinical use is still in the early stages[220].

3.4 : Simulation:

3.4.1 Simulation Process Steps:

Simulations require a few steps, including setting up the geometry and mesh, processing the data, running the calculations, and postprocessing the results.

1) Geometry:

Creating a 3d representation of an object under study utilizing plans and drawings

2) Mesh Creation:

The process involves partitioning the pre-existing 3-dimensional model into a vast number of discrete numerical elements. Stated differently, it refers to the process of dividing the numerical space into discrete units. Thus, in the process of computation, it is assumed that all computed variables remain constant within the element.

3) Pre-Processing:

For use in the computation, physical model, property, initial, and boundary condition definitions are provided.

4) Calculation:

The variables in each numerical element are repeatedly calculated while taking the boundary conditions into consideration.

5) Post-Processing:

Interpreting scalar or vector regions of variables; evaluating values at the surface and volume integrals; generating streamline, surface, and contour charts.

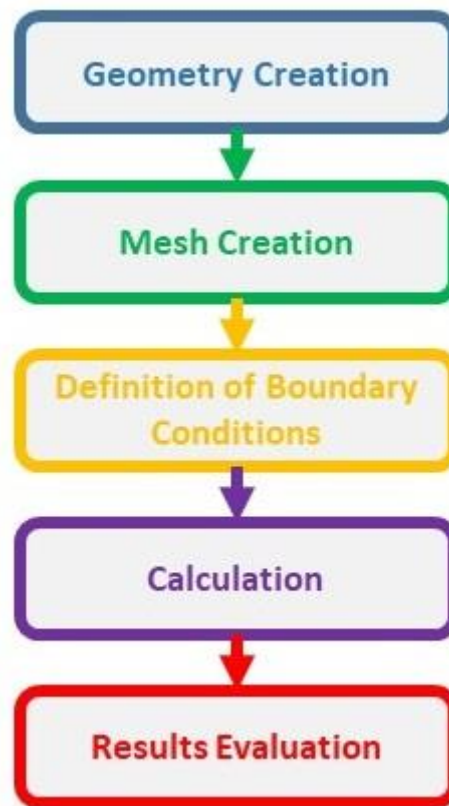


Figure 03.12: CFD-Simulation Process

3.4.2 Finite Element Method (FEM):

FEM is a numerical technique that uses finite elements to discretize the problem domain and solve the governing equations. It is widely used in engineering to solve problems with complex geometries, material properties, and boundary conditions. It can be used for structural analysis of both solids and fluids. However, the accuracy of the FEM solution depends on the mesh density and quality, and it is more reliable than FVM[221]. The finite element approach, in contrast to the finite volume method, might take longer to solve problems[222].

3.4.3 Finite Volume Method (FVM):

FVM is based on the conservation law principles like mass-energy and approximates the integral form of the governing equations including Navier-Stokes using fluxes across the boundaries of control volumes. This makes FVM a memory-efficient and

computationally efficient method for solving complex fluid flow problems. FVM is also known to handle discontinuities in the solution better and more rapidly than some other methods [223].

3.4.4 Boundary Element Method (BEM):

Instead of discretizing the entire domain, BEM only discretizes the boundary of the domain and computes the solution at the boundary. This approach reduces the dimensionality of the problem and makes it easier to solve, particularly for problems with complicated geometries[224].

BEM works by dividing the boundary into small segments, called boundary elements. The solution at each element is represented by a set of basic functions, typically singular or fundamental solutions to the governing partial differential equations (PDEs)[225]. The boundary element method then uses Green's theorem to convert the problem into a set of linear equations that can be solved numerically.

3.4.5 Finite Difference Method (FDM):

In addition to being easily programmable, the finite difference approach is historically significant. Integrated boundaries or overlapping meshes allow these few specialized algorithms to handle complicated geometry with precision and performance.

Chapter 4

Materials and Methods

4.1 Problem Statement:

As stated before, bone is an important part of the human body that is responsible for its shape and providing mechanical support. Despite the bone's natural ability to heal, bone injuries and fractures still pose a huge problem for humans in older ages and especially in cases where bone regrowth is required in large scale.

To resolve these issues, external implants, and bone graft substitutes (metal rods, bio-ceramic based scaffolds) are prepared to repair bone defects.

But there is still need of high-performance scaffolds that meets the design criteria for ideal scaffold.

The ideal scaffold must acquire the following properties all of which stimulate the rapid regeneration of bones.

- i.** Biocompatible and nontoxic.
- ii.** A reliable drug delivery system (controlled delivery of drug)
- iii.** Hydrophobic.
- iv.** Highly porous

First of all scaffold should be biocompatible to avoid any possible cytotoxicity, immunotoxicity, and immune responses from the body[226].The ways that drugs are incorporated, the qualities of the polymer, the process used to produce the scaffold, the number of layers, and porous architectures, among other factors, can all affect how quickly drugs are released into the body. Scaffolds should provide structural support to bone that is essential for guided bone regeneration. For this purpose, scaffolds should be hydrophobic because they are not dissolved in water therefore their strength is not compromised.

4.2 Materials:

Material used included.

- 1) PAN (Polyacrylonitrile)
- 2) PICT (Poly I,4 Cyclohexane Di-methylene Isosorbide Terephthalate)
- 3) ZnO (Zinc Oxide)
- 4) SiO₂ (Silicone Dioxide)
- 5) CaO (Calcium Oxide)
- 6) HA (Hydroxyapatite)
- 7) TFA (Trifluoroacetic acid)
- 8) CF (Chloroform)
- 9) DMF (Dimethylformamide)

we obtained these materials from various vendors around the world.

Polyacrylonitrile (PAN):

PAN (Polyacrylonitrile) With Average Molecular Weight 150,000 Was Supplied by Sigma-Aldrich Corporation (Saint Louis, MO 63103, USA).

PAN Is a synthetic polymer with *Acrylonitrile* as the main component. PAN is a good candidate for tissue regeneration due to high conductivity and biocompatibility. It is a versatile polymer used to make products, including fibers for textiles (Orlon), ultra-filtration membranes ,hollow fibers for water filtration (techniques like RO) and primary precursor for high-quality carbon fibers.

Table 4.0-2: Properties of PAN

property	values
IUPAC Name	Polyacrylonitrile
Chemical Formula	(C ₃ H ₃ N) _n
Appearance	White Solid
T _m	325°C

Softening Point	190-240°C
Tg	95°C
Density	1.184 g/cm ³
Solubility In Water	Insoluble
Elongation	25-50%
Abrasive Resistance	Good

In 1971 Baumgarten was the first to use polyacrylonitrile/dimethylformamide (PAN/DMF) solution, which was ejected from a metal capillary.

PICT:

“PICT” also known as “SKYPURA” Poly(1,4 Cyclohexane Dimethylene Isosorbide Terephthalate) (Mw \approx 46800g/Mol) in pallets form was supplied by SK Chemicals, Korea).SKYPURA” is the Korea’s first PCT-based material for super engineering plastic. The product displays exceptional chemical resistance, reflexivity, durability and stabilized insulation, which makes it an optimal material for electrical and electronic components. PICT won the minister’s prize at the 2013 Korea Technology Awards hosted by the Ministry of Trade, Industry and Energy.

Trifluoroacetic Acid (TFA):

TFA (Acid) 99.9% pure was procured from Fujitsu Pure Chemical (Wako).while Dimethylformamide (DMF) was supplied by FUJIFILM Wako Pure Chemical Corporation Osaka, Japan.

Trifluoroacetic acid (TFA) is a highly polar solvent with a variety of unique properties that make it an excellent choice for many applications in chemistry. One of the most significant factors contributing to TFA's usefulness as a solvent is its high polarity. Fluorine has a very high electronegative character, as a result it pulls the bonded pair of electrons towards itself, thus making the O-H bond weak and hence, it

easily loses the hydrogen as H⁺, thus making it a stronger acid than acetic acid, where there is no such electronegative group attached to carbon.

The appreciated property of TFA is that it is highly volatile therefore it evaporates within seconds during electrospinning process as fiber jet travels from needle to collector.

Hydroxyapatite (HA):

Hydroxyapatite nanoparticles (HANPs) are incorporated in the core of all scaffolds. The properties of (HANPs) are listed in the table below.

Table 4.0-3: Properties of HA

Property	Values
Poisson's Ratio	0.27
Bioactivity	High
Biodegradation	Low
Cellular Compatibility	High
Young's (Elastic) Modulus	35–120 GPa
Fracture Energy	2.3–20 J/M ² (Brittle Ceramic)
Biocompatibility	High

Calcium oxide (CaO):

Calcium oxide (CaO NPs) are incorporated in shell of all three scaffolds. The properties of CaO NPs are given in the table below.

Table 4.0-4: Properties of CaO

Property	Values
IUPAC Name	Oxocalcium
Molecular Weight	56.0768 g/mol
Density	3.35 g/cm ³
Porosity	0.5%
Color	White / pale yellow
Surface Area	4 cm ² /g
Cellular Compatibility	High
Antimicrobial Activity	High
Toxicity	Low
Biodegradation	Low

Silicon Dioxide SiO₂:

Silicon Dioxide nanoparticles (SiO₂NPs) are incorporated in the core of all three scaffolds due to their higher biocompatibility. The properties are given in the table below.

Table 4.0-5: Properties of SiO²

Property	Values
Density	32.2 gm/cm ³
Elastic Modulus	71.7 GPa
Tensile Strength	48.3 MPa
Density	2.18g/cm ³
Poissons Ratio	0.17
Crystal Structure	Amorphous
Melting Temperature	1700 °C
Hardness	2600 Kg/mm ²

Zinc oxide (ZnO):

Zinc oxide/ZnO NPs are being used for many biomedical applications. Here below are some of its properties.

Table 4.0-6: Properties ZnO

Property	Values
Molar Mass	81.408 g/mol
Melting Point	1974 c°
Poisson's Ratio	0.25
Density	5.606 g/cm ³
Youngs Modulus	108 GPa
Surface Area	48.09 m ² g ⁻¹
Biocompatibility	High
Toxicity	Low
Antibacterial Activity	High
Bonding Capability	High

4.3 Methodology:

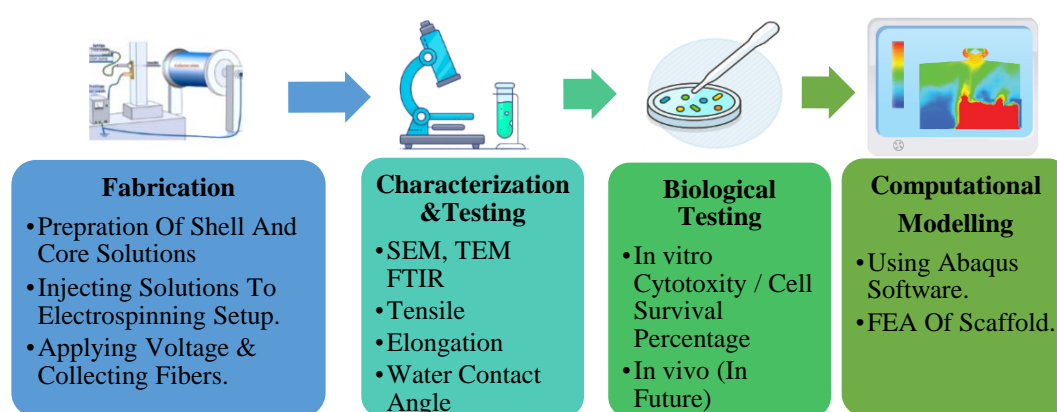


Figure 4.13: Scheme of Development of Nano Fibrous Scaffold

4.4 Fabrication of Core and Shell Nanofibers:

The nano fabric is non-woven like diapers, facemask & teabags. The main advantage of nonwovens is that they can be mass produced.

Three nonwoven nano fibrous scaffolds of different composition were fabricated by using electrospinning machine(name/model). Each nanofiber is coaxial, that means each fiber has a well-defined ‘*CORE & SHELL.*’

Table 4.0-7: Composition of all Scaffolds

	SHELL			CORE		
	PICT(const)	CaO(const)	SiO ₂	PAN (const)	ZnO (const)	HA
1 st Coaxial Fiber	10%	3%	1.5%	10%	1.5%	3%
2 nd Coaxial Fiber	10%	3%	3%	10%	1.5%	4.5%
3 rd Coaxial Fiber	10%	3%	4.5%	10%	1.5%	6%

$$\text{COAXIAL FIBER} = \text{CORE} + \text{SHELL}$$

The purpose of fabricating three nanofibers was to choose the best performing and feasible scaffold for bone support and bone regeneration. The technique used for fabrication of coaxial nanofibers is “Electrospinning”.

The reason for choosing electrospinning technique offers precise control over fiber diameter, high surface area-to-volume ratio, versatility, and scalability, making it useful in many fields including tissue engineering, drug delivery, and filtration. This

technique uses simple physical manufacturing process hence no need for complex chemical reactions.

To test the spinnability of polymers and nanoparticles/drugs only 1-gram solutions of each shell and core were prepared. These samples were stirred at prepared in the same conditions as full scale solutions. This was repeated for all three scaffolds.

4.4.1 1st coaxial Nano fibrous Scaffold:

For each nanofiber two different solutions were prepared, one for Core and the other for Shell.

a) Preparation of Shell Solution:

10-gram shell solution is prepared by using **2 solvents** (TFA, Chloroform) & **3 solutes** (PICT, CaO, SiO₂). The composition of shell solution is measured by the method below.

PICT(const)	CaO(const)	SiO ₂	TFA	CF
10%	3%	1.5%	25%	75%

Weight of 10% PICT = 1 gram

Weight of 3% CaO = 0.3 grams

Weight of 1.5% SiO₂ = 0.15 grams

Total weight of solute = wt. of PICT + wt. of CaO + wt. of SiO₂

$$= 1 \text{ gram} + 0.3 \text{ grams} + 0.15 \text{ grams}$$

Total weight of solute = 1.45 grams

Now, we calculate the weights of solvents.

Total weight of solvent = wt. of solution – wt. of solute

$$= 10 \text{ gram} - 1.45 \text{ gram}$$

Total weight of solvent = 8.55 grams

$$\text{Wt. of TFA} = \frac{25}{100} \times 8.55$$

$$\text{Wt. of TFA} = 2.125 \text{ grams}$$

$$\text{Wt. of CF} = \frac{75}{100} \times 8.55$$

$$\text{Wt. of CF} = 6.412 \text{ grams}$$

Table 4.0-8: Composition of 1st shell solution

Materials	Weight (grams)
PICT 10% (const)	1
CaO 3% (const)	0.3
SiO ₂ 1.5%	0.15
Total Solute	1.45
TFA 25% of Solvent	2.125
Chloroform 75% of Solvent	6.412
Total solvent	8.55

b) Preparation of Core Solution:

By using the same method used to make shell solution. We prepared a 10g core solution. While using DMF as solvent. The percentage composition of each material is given as below.

PAN (const)	ZnO (const)	HA
10%	1.5%	3%

$$\text{Wt. of PAN} = 1 \text{ grams}$$

Wt. of ZnO = 0.15 grams

Wt. of HA = 0.3 grams

Total weight of solute = 1.45

For core, only DMF is used as solvent. Therefore,

Total weight of solvent/DMF = 10 - 1.45

Total weight of solvent/DMF = 8.55 grams

Table 4.0-9: Composition of 1st core solution

Materials	Weight (grams)
PAN 10% (const.)	1
ZnO 1.5% (const.)	0.15
HA 3%	0.3
Total Solute	1.45
Total Solvent/ DMF	8.55

4.4.2 2nd coaxial Nano fibrous Scaffold:

Preparation of Shell Solution:

10-gram shell solution is prepared, and the composition of shell solution is measured by the method below.

PICT(const)	CaO(const)	SiO₂	TFA	CF
10%	3%	3%	25%	75%

Weight of 10% PICT = 1 gram

Weight of 3% CaO = 0.3 grams

$$\text{Weight of 3\% SiO}_2 = 0.3 \text{ grams}$$

$$\begin{aligned} \text{Total weight of solute} &= \text{wt. of PICT} + \text{wt. of CaO} + \text{wt. of SiO}_2 \\ &= 1 \text{ gram} + 0.3 \text{ grams} + 0.3 \text{ grams} \end{aligned}$$

$$\text{Total weight of solute} = 1.6 \text{ grams}$$

Now, we calculate the weights of solvents.

$$\begin{aligned} \text{Total weight of solvent} &= \text{wt. of solution} - \text{wt. of solute} \\ &= 10 \text{ gram} - 1.6 \text{ gram} \end{aligned}$$

$$\text{Total weight of solvent} = 8.4 \text{ grams}$$

$$\text{Wt. of TFA} = \frac{25}{100} \times 8.4$$

$$\text{Wt. of TFA} = 2.1 \text{ grams}$$

$$\text{Wt. of CF} = \frac{75}{100} \times 8.4$$

$$\text{Wt. of CF} = 6.3 \text{ grams}$$

Table 4.0-10: Composition of 2nd Shell Solution

Materials	Weight (grams)
PICT 10% (const)	1
CaO 3% (const)	0.3
SiO ₂ 3 %	0.3
Total Solute	1.6
TFA 25% of Solvent	2.1
Chloroform 75% of Solvent	6.3
Total solvent	8.4

All weighted materials stirred/mixed together for 3 hours at room temperature on magnetic stirrer to form homogenous solution.

Preparation of Core Solution:

By using the same method used to make shell solution. We prepared a 10g core solution. While using DMF as solvent. The percentage composition of each material is given as below.

PAN (const)	ZnO (const)	HA
10%	1.5%	4.5%

While DMF used as solvent in core solution to dissolve PAN.

Wt. of PAN = 1 grams

Wt. of ZnO = 0.15 grams

Wt. of HA = 0.45 grams

Total weight of solute = 1.6

For core, only DMF is used as solvent. Therefore,

Total weight of solvent/DMF = 10 – 1.6

Total weight of solvent/DMF = 8.4 grams

Table 4.0-11: Composition of 2nd Core Solution

Materials	Weight (grams)
PAN 10% (const.)	1
ZnO 1.5% (const.)	0.15
HA 4.5%	0.45
Total Solute	1.6
Total Solvent/ DMF	8.4

4.4.3 3rd coaxial Nanofibrous Scaffold:

PICT(const)	CaO(const)	SiO ₂	TFA	CF
10%	3%	4.5%	25%	75%

$$\text{Weight of 10\% PICT} = 1 \text{ gram}$$

$$\text{Weight of 3\% CaO} = 0.3 \text{ grams}$$

$$\text{Weight of 4.5\% SiO}_2 = 0.45 \text{ grams}$$

$$\begin{aligned} \text{Total weight of solute} &= \text{wt. of PICT} + \text{wt. of CaO} + \text{wt. of SiO}_2 \\ &= 1 \text{ gram} + 0.3 \text{ grams} + 0.45 \text{ grams} \end{aligned}$$

$$\text{Total weight of solute} = 1.75 \text{ grams}$$

Now, we calculate the weights of solvents.

$$\begin{aligned} \text{Total weight of solvent} &= \text{wt. of solution} - \text{wt. of solute} \\ &= 10 \text{ gram} - 1.75 \text{ gram} \end{aligned}$$

$$\text{Total weight of solvent} = 8.25 \text{ grams}$$

$$\text{Wt. of TFA} = \frac{25}{100} \times 8.25$$

$$\text{Wt. of TFA} = 2.06 \text{ grams}$$

$$\text{Wt. of CF} = \frac{75}{100} \times 8.25$$

$$\text{Wt. of CF} = 6.19 \text{ grams}$$

Materials	Weight (grams)
PICT 10% (const)	1
CaO 3% (const)	0.3
SiO₂ 4.5 %	0.45
Total Solute	1.75
TFA 25% of Solvent	2.06
Chloroform 75% of Solvent	6.19
Total solvent	8.25

Table 4.0-12: Composition of 3rd Shell Solution

All weighted materials stirred/mixed together for 3 hours at room temperature on magnetic stirrer to form homogenous solution.

Preparation of Core Solution:

PAN (const)	ZnO (const)	HA
10%	1.5%	6%

By using the same method used to make shell solution. We prepared a 10g core solution, while using DMF as solvent. The percentage composition of each material is given as below.

Wt. of PAN = 1 grams

Wt. of ZnO = 0.15 grams

Wt. of HA = 0.6 grams

Total weight of solute = 1.75

For core, only DMF is used as solvent. Therefore,

Total weight of solvent/DMF = 10 – 1.75

Total weight of solvent/DMF = 8.25 grams

Table 4.0-13: Composition of 3rd Core Solution

Materials	Weight (grams)
PAN 10% (const.)	1
ZnO 1.5% (const.)	0.15
HA 6%	0.6
Total Solute	1.75
Total Solvent/ DMF	8.25

After weighing all the precursors and nanoparticles precisely. The core and shell solutions for each nanofiber were stirred in two separate reagent bottles. both core and shell solutions of each nanofiber were prepared and stirred at same time.

4.5 Characterization and Testing

4.5.1 Introduction to FTIR:

FTIR spectroscopy is a very effective analytical technique used in chemistry, physics, and materials science. It involves the study of the vibrational modes of molecules in the infrared region of the electromagnetic spectrum. The FTIR spectrum provides a unique "fingerprint" of the sample, It may be used for identification of unknown compounds or monitor chemical reactions. FTIR has numerous applications, including the identification of unknown compounds[227], the analysis of polymers and plastics, the characterization of pharmaceuticals, and the monitoring of chemical reactions.

FTIR spectroscopy operates on the fundamental principle of a sample's absorption or transmission of infrared radiation. Infrared radiation refers to a type of

electromagnetic radiation that has wavelengths that are longer than those of visible light, but shorter than those of radio waves. When infrared radiation is passed through a sample, it interacts with the molecular vibrations within the sample, leading to the absorption or transmission of the radiation at certain wavelengths. The FTIR spectrometer then measures the intensity of the absorbed or transmitted radiation as a function of wavelength[228].

4.5.1.1 Preparation of Sample and Analysis:

The procedure for performing FTIR spectroscopy involves several steps. Firstly, the sample is prepared, which may involve making a thin film . The sample must be transparent to infrared radiation to allow the radiation to pass through and interact with the molecular vibrations within the sample. The prepared sample is then placed in the sample holder of the FTIR spectrometer.

Secondly, the instrument is set up to measure the infrared beam intensity as a function of wavelength. This involves calibration of the instrument, including the adjustment of various optical components such as mirrors and filters. Once the instrument is properly calibrated, the sample is scanned with the infrared beam, and the intensity of the transmitted or absorbed beam is measured at different wavelengths. This process is repeated multiple times to obtain an accurate and reproducible spectrum. many studies used FTIR to analyze the mineralization of bone regeneration process[229].

4.5.2 Introduction to TEM:

The Transmission Electron Microscopy (TEM) technique is highly effective in producing detailed images of samples by utilizing an electron beam. This imaging technique offers a comprehensive view of the atomic-level structure of the materials. The procedure involves preparing the sample, setting up the instrument, acquiring the data, and processing the image. The Transmission Electron Microscope (TEM) is a commonly utilized tool in both materials' science and biological research. It offers a comprehensive analysis of the atomic-scale structure and composition of materials.

The operation of TEM is based on the interaction of electrons with matter. In a TEM, a beam of electrons is generated by an electron gun, which typically uses a tungsten filament to heat and emit electrons. The sample is exposed to an electron beam that is

precisely focused using a set of electromagnetic lenses. These lenses can be fine-tuned to regulate the beam's size and intensity. As the electron beam passes through the sample, some of the electrons are scattered or absorbed by the atoms and structures in the sample. The electrons that are dispersed are detected and utilized to create an image of the specimen. The generation of the image involves the alteration of the electron beam's intensity and the subsequent measurement of the scattered electrons' intensity at each point.

4.5.2.1 Preparation of Sample and Analysis:

The sample for TEM is typically an ultra-thin film of fabric, usually less than 100 nanometers thick, which is placed on a thin support grid. The sample must be transparent to electrons and prepared in a way that preserves its internal structure. Depending on the sample, this may involve cutting, polishing, and chemical treatments.

Once the data has been collected, it is processed using specialized software to generate the final image. The image can be adjusted to enhance contrast and remove noise, and different imaging modes can be used to provide additional information about the sample.

Materials as diverse as metals, polymers, and even biological material may all benefit from the in-depth analysis made possible by transmission electron microscopy (TEM). It is commonly used in materials science, nanotechnology, and biological research to study the properties and behavior of materials at the atomic scale.

4.5.3 Introduction to Water Contact Angle:

The water contact angle is the angular separation between a solid's surface and a water droplet in contact with that surface. It is a fundamental parameter in identifying the wetting behavior of materials and their hydrophobicity, or water-repelling ability.

A goniometer, a device that measures the angle between a surface and a droplet of water, is commonly used to measure the water contact angle. Using a goniometer, we can determine the angle between the droplet's tangent to the surface at the contact point and the droplet's tangent to the surface at the three-phase contact line. In 1800s

Young presented water contact angle theory and put forward its equation[230] stated below.

$$\gamma_{SG} = \gamma_{SL} + \gamma_{LG} \cos(\theta_C)$$

The principal value of the equation resides in its capacity to describe surface wetting processes and provide an approximation of the tension across the surface of a solid, both of which are extremely useful pieces of knowledge to have on record[231]. The measurement of water contact angle can range from 0° to 180°, depending on the wetting properties of the sample. A contact angle of 0° indicates that the droplet fully wets the surface and spreads out in a thin film. A droplet assumes a spherical shape and does not moisten the outermost layer at all when the contact angle is 180 degrees. A material with a high-water contact angle, typically greater than 90°, is said to be hydrophobic or water-repelling. This is because the surface is able to resist the spreading of the droplet and cause it to bead up and roll off, like on a lotus leaf. In contrast, a material with a low water contact angle, typically less than 90°, is said to be hydrophilic or water-attracting. This is because the surface allows the droplet to spread out and wet the surface.

The effect of water contact angle on hydrophobicity is significant in many applications, such as in coatings and surface treatments. Materials with high water contact angles are desirable for their water-repelling properties, which can improve the durability and longevity of products. For example, hydrophobic coatings can be used to protect buildings from water damage, or to create water-resistant textiles for outdoor apparel[232].

In summary, the water contact angle is a measurement of the angle between the surface of a material and a droplet of water in contact with it. When the contact angle is high, the surface is hydrophobic, and when it's low, the surface is hydrophilic. Understanding the wetting characteristics of materials requires consideration of the water contact angle, and it has significant applications in coatings and surface treatments.

4.5.4 Introduction to SEM:

The scanning electron microscope (SEM) is a cutting-edge, versatile equipment often used to study material surfaces. High-resolution photographs of the topography and morphology of a sample's surface may be obtained using SEM, an imaging method that employs a concentrated beam of electrons to scan the outermost layer of the sample [233]. The operation of SEM is based on the interaction of electrons with matter. In SEM, an electron beam is generated by an electron gun, which typically uses a tungsten filament to heat and emit electrons. After that, the electron beam is directed towards the specimen using a series of electromagnetic lenses, which can be adjusted to control the size and intensity of the beam.

Major Components of SEM Technique:

- A device that generates an electron beam
- Electrons in motion via electromagnetic lenses that descend in a column.
- A device that can detect an electron beam.
- We put the sample into the sample chamber.
- Finally, the computer displays the findings and the pictures.

When the sample is exposed to the electron beam, it generates different types of signals, including secondary electrons, backscattered electrons, and X-rays. These signals carry information about the topography, morphology, and composition of the sample, and are detected by special detectors. The most common detector used in SEM is the Everhart-Thornley detector, which detects secondary electrons. When the main electron beam collides with the sample surface, secondary electrons are released, causing some of the surface electrons to be ejected. The detector picks up on the path of these propelled electrons to create a digital image of the material.

Backscattered electrons, on the other hand, are electrons that are scattered back in the direction of the electron beam. These electrons are detected by a different detector, called the In-lens detector, and can provide information about the atomic number and density of the sample. In addition to detecting secondary and backscattered electrons, SEM can also generate X-rays, which can provide information about the chemical composition of the sample.

The final image generated by SEM is a two-dimensional representation of the surface of the sample, with different shades of gray or color representing variations in the intensity of the detected signals. The image can be further processed using specialized software to enhance contrast, remove noise, and provide additional information about the sample[234].

The Scanning Electron Microscope (SEM) is a highly effective imaging technique that finds extensive application in the fields of materials science, nanotechnology, and biological research. It offers comprehensive insights into the structure and composition of materials at the micro- and nanoscale. To obtain accurate images using SEM, the sample must be coated with a conductive material like gold or carbon. This is necessary to prevent any charge buildup that could potentially distort the image. Once the data has been collected, it is processed using specialized software to generate the final image.

4.6 Modeling & Simulation using FEM:

Finite Element Method (FEM) is a powerful numerical technique used in engineering and design. It is highly applicable in cross disciplines including its application in fabric design, analysis and development. It allows for the simulation and analysis of complex structures by dividing them into smaller, manageable elements.

In this particular study, FEM is employed to study fabric mechanical behavior, predict its performance, and forecast its design optimization. By discretizing the complex fabric structure into smaller elements, such as triangles or quadrilaterals, enable us accurate analysis of their mechanical properties. We have utilized this technique to understand how the fabric will respond to different stresses and strains. Fabric designers and engineers can effectively utilize this method for fabric structures by iteratively refining the element arrangement, material properties, and geometric configurations. This optimization process can lead to improved fabric performance, such as enhanced tensile strength, tear resistance, or flexibility.

We have produced some tangible results, that will aid in virtual prototyping, allowing designers to evaluate fabric performance before physical manufacturing. This saves time and resources by identifying potential issues early in the design process and facilitating informed design decisions.

Abaqus CAE is used for this particular simulation. Abaqus CAE is a powerful suite widely used in engineering and research for simulating and analyzing the behavior of complex structures. It is developed and maintained by Dassault Systèmes, a leading provider of 3D design and simulation software.

It employs advanced numerical solution algorithms, such as implicit and explicit solvers, to efficiently solve the system of equations generated by the finite element analysis. These solvers are designed to handle large-scale problems and can utilize parallel processing for improved computational efficiency.

4.6.1 Simulation Process Steps:

Simulations require a few steps, including setting up the geometry and mesh, processing the data, running the calculations, and post processing the results. A comprehensive analysis of a newly developed fabric, focusing on the simulation of its tensile strength and the development of von Mises stress within the material.

i. Geometry:

The first issue faced when creating a FEM is what level of morphological complexity should or can the model reflect, and how can appropriate morphology be captured for the digital environment. A simple geometry therefore was created using 3D extrusion to generate mesh and apply required boundary conditions.

ii. Mesh Creation:

The process involves partitioning the pre-existing 3-dimensional model into a vast number of discrete numerical elements. Stated differently, it refers to the process of dividing the numerical space into discrete units. Thus, in the process of computation, it is assumed that all computed variables remain constant within the element.

iii. Pre-Processing:

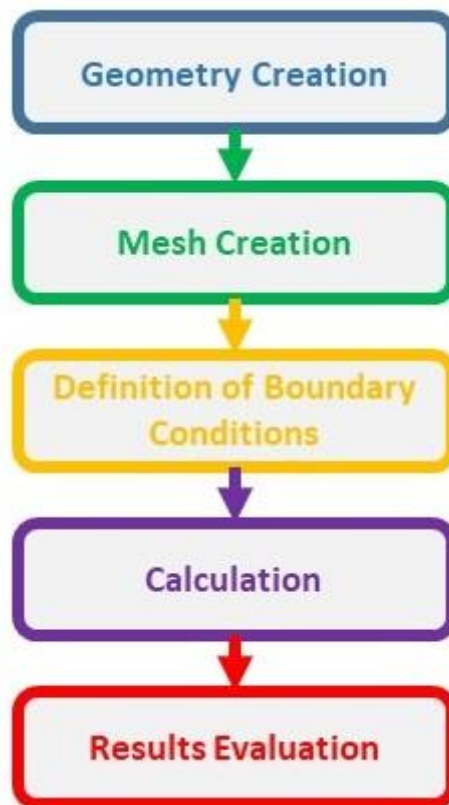
For use in the computation, physical model, property, initial, and boundary condition definitions are provided.

iv. Calculation:

The variables in each numerical element are repeatedly calculated while taking the boundary conditions into consideration (Refer to results chapter).

v. Post-Processing:

Interpreting scalar or vector regions of variables; evaluating values at the surface and volume integrals; generating streamline, surface, and contour charts (Refer to results chapter)



4.6.2 Modeling of Scaffold:

To simplify the simulation process and mitigate mesh complexities, the fabric geometry was represented as a cylindrical shape, with a diameter of 200 nanometers, equivalent to the thickness of a single fabric fiber. The boundary conditions were defined as follows: one end of the fabric was fixed, while a displacement of 0.01 mm

was applied to the other end. By employing this simplified geometry, accurate insights into the fabric's behavior under tensile loading could be obtained.

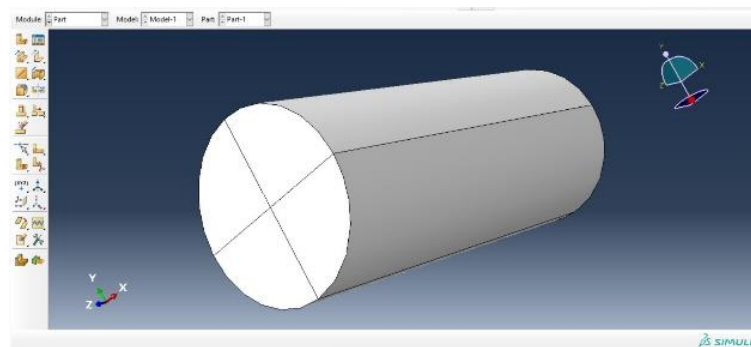


Figure 4.14

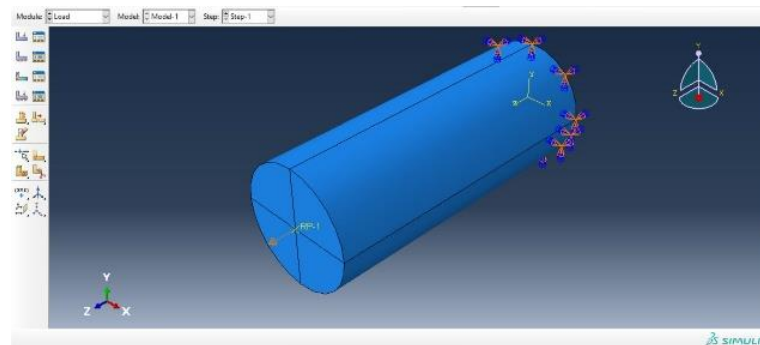


Figure 4.15

The material properties utilized in the simulation were derived from experimental data. The fabric exhibited a Young's modulus of 0.1879 MPa, indicating its stiffness, and a Poisson's ratio of 0.2, representing its resistance to lateral strain. Additionally, the fabric's density was determined to be $1.184e-9$ tons/mm³, uniformly distributed across the entire geometry.

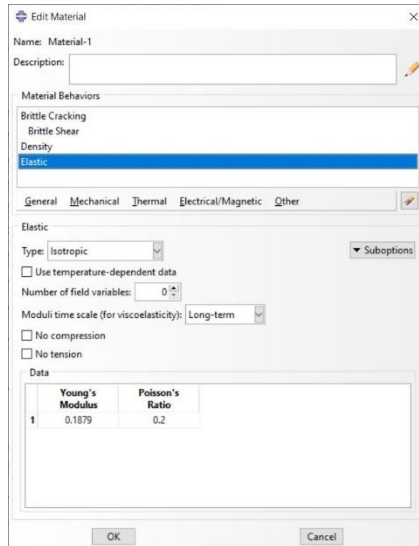


Figure 04.16

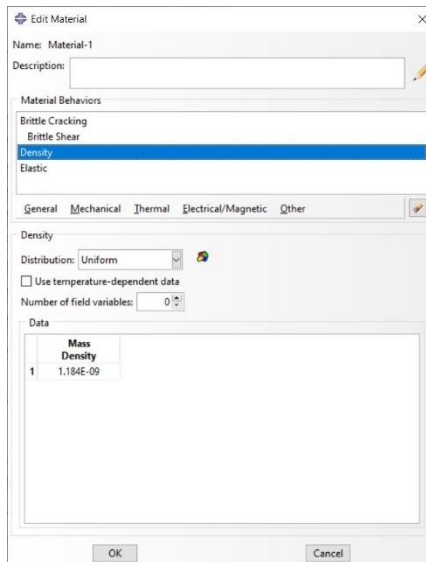


Figure 4.17

The chosen material model for this simulation was the brittle cracking model, which accurately captured the behavior of the fabric when subjected to tensile forces. The model incorporated a direct cracking strain, as illustrated in Figure 4.7. Furthermore, shear retention factor and crack opening strain were defined, as outlined in Figure 4.6, to provide a comprehensive representation of the fabric's failure characteristics.

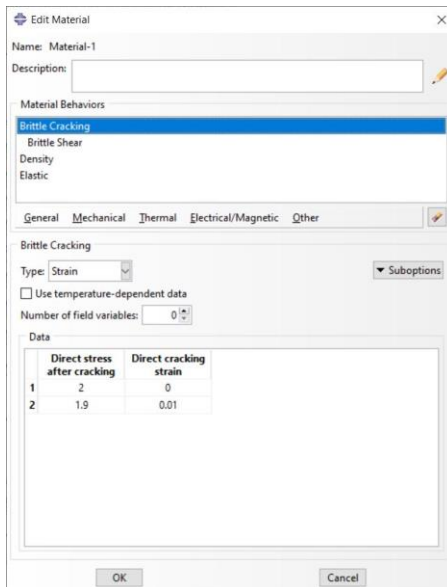


Figure 04.18

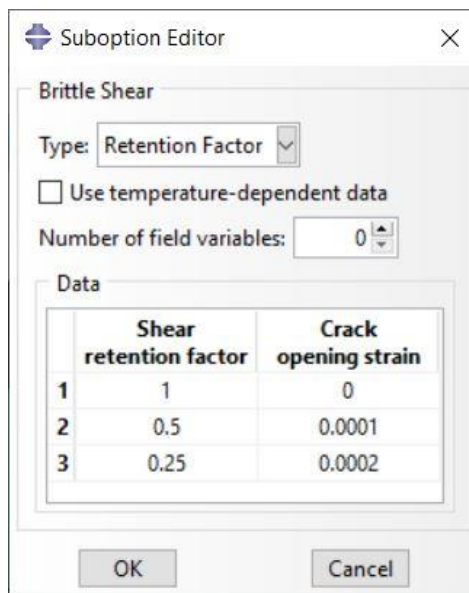


Figure 4.19

The geometry was discretized using quad elements, resulting in 26,789 elements and 28,601 nodes in total. To ensure accurate representation, a fine structured mesh was employed, with a mesh size of 1 nm, effectively capturing the intricate details of the fabric's behavior during simulation.

```
NUMBER OF ELEMENTS IS                26789
NUMBER OF NODES IS                   28601
NUMBER OF NODES DEFINED BY THE USER  28601
TOTAL NUMBER OF VARIABLES IN THE MODEL 87756
(DEGREES OF FREEDOM PLUS MAX NO. OF ANY LAGRANGE MULTIPLIER
VARIABLES. INCLUDE *PRINT,SOLVE=YES TO GET THE ACTUAL NUMBER.)
```

Figure 4.20

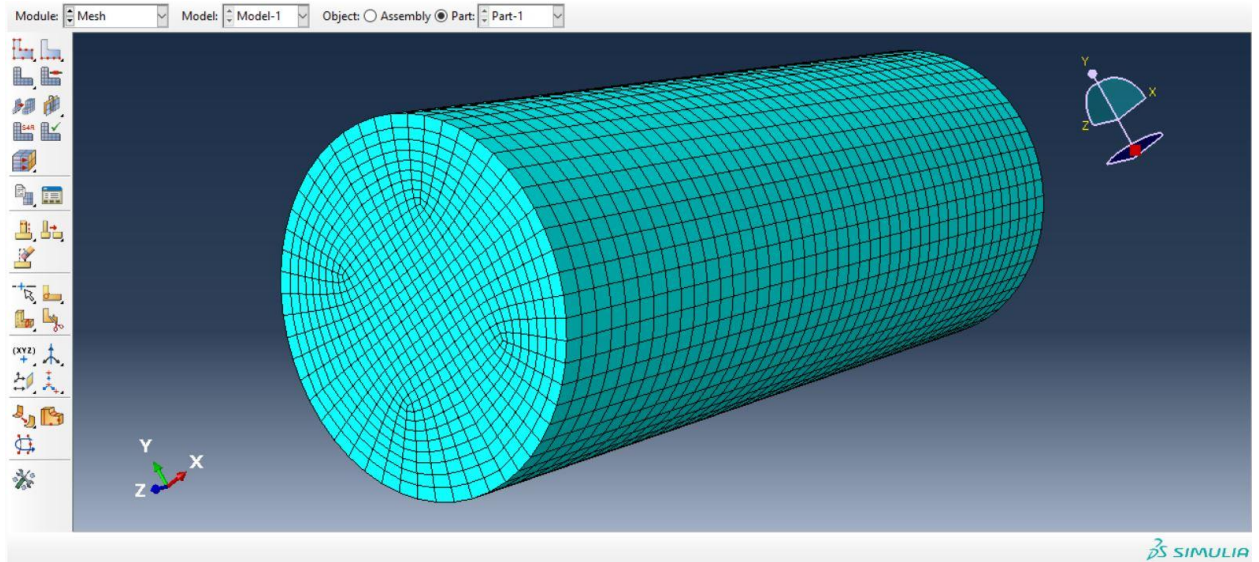


Figure 4.21

It should be kept in mind that there can always be a chance of error while doing Finite element modelling which could be analytical, numerical, or experimental, or might be combination of all of them.

Solutions to these errors are based on scientific approximations, in making a decision for selection of a specific decision we should have additional information about the problem, for example its coherency with results from other comparative models. The results of the fabric simulation are explained in chapter 5 (Results and Discussions).

Chapter 5

Result and Discussion

In this chapter, we examined a nanofibrous scaffold through testing, characterization, and simulation. Various techniques were used to evaluate its performance, morphology, and mechanical properties.

In vitro cytotoxicity testing assessed the scaffold's biocompatibility with living cells. Scanning electron microscopy and transmission electron microscopy provided surface and internal structure images, respectively. Tensile testing measured mechanical parameters like young's modulus strength and elasticity. Wettability behavior analysis determined the scaffold's interaction with liquids, while FTIR analysis identified its chemical composition. Simulation using FEM analyzed the scaffold's mechanical behavior under same conditions as provided in physical lab.

By combining these techniques, we gained a comprehensive understanding of the scaffold's properties, enabling further development and potential applications in tissue engineering.

5.1 Invitro Cytotoxicity:

The toxicity potential of the resultant nanofibers-based scaffolds was investigated through in-vitro assessment. By following this comprehensive methodology, the toxicity potential of the nanofibers-based scaffolds was evaluated through in-vitro assessment using Line L929 cells. The study employed Line L929 cells as a representative cell line and involved a 72-hour evaluation period. Each sample and cell line were subjected to triplicate testing to ensure the reliability and accuracy of the results. Before conducting the assessment, the samples underwent sterilization. Once sterilization was completed, the samples were cultured in DMEM/F12 medium for 72 hours. The cell viability, indicative of toxicity potential, was calculated as a percentage relative to the negative control.

At the end of the 72-hour assessment period, 15% of the medium culture containing Thiazolyl Blue Tetrazolium Bromide (MTT; 5mg/ml) was added to each well. The samples were then incubated at 37°C with 5% CO₂ for 5 hours. Following this

incubation, the medium was carefully removed, and the samples were washed with phosphate-buffered saline (PBS).

To quantify cell viability, the Formosan crystals resulting from MTT metabolism by viable cells were dissolved in 400 μ l of dimethyl sulfoxide (DMSO). Subsequently, 200 μ l of each solution was transferred to new 96-well plates, and the absorbance was measured at 570 nm using a spectrophotometer. To determine the contribution of the scaffolds themselves to the dye absorption, control samples without any cells were immersed in the medium culture containing MTT. These control samples were subjected to the same washing and measurement procedures as the cell-containing samples. The absorbance readings at 570 nm for the control samples allowed the measurement of dye absorption by the scaffolds alone.

To estimate the number of cells adhering to the scaffolds, the absorbance resulting from the scaffolds' dye absorption was subtracted from the absorbance measured in the presence of the L929 cell line. This subtraction effectively eliminated the contribution of the scaffolds' inherent dye absorption, allowing for a more accurate determination of cell adhesion. The calculations and measurements carried out provided valuable insights into the cell viability and adhesion characteristics of the scaffolds, contributing to a better understanding of their biocompatibility and potential for use in various biomedical applications.

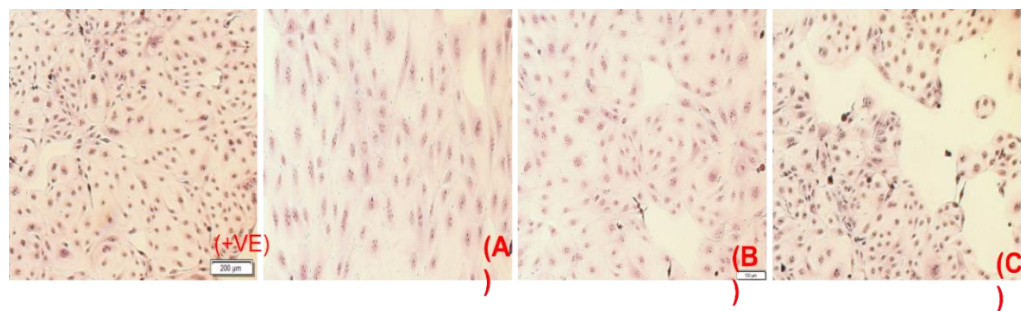


Figure 5.22: Images For Invitro Study

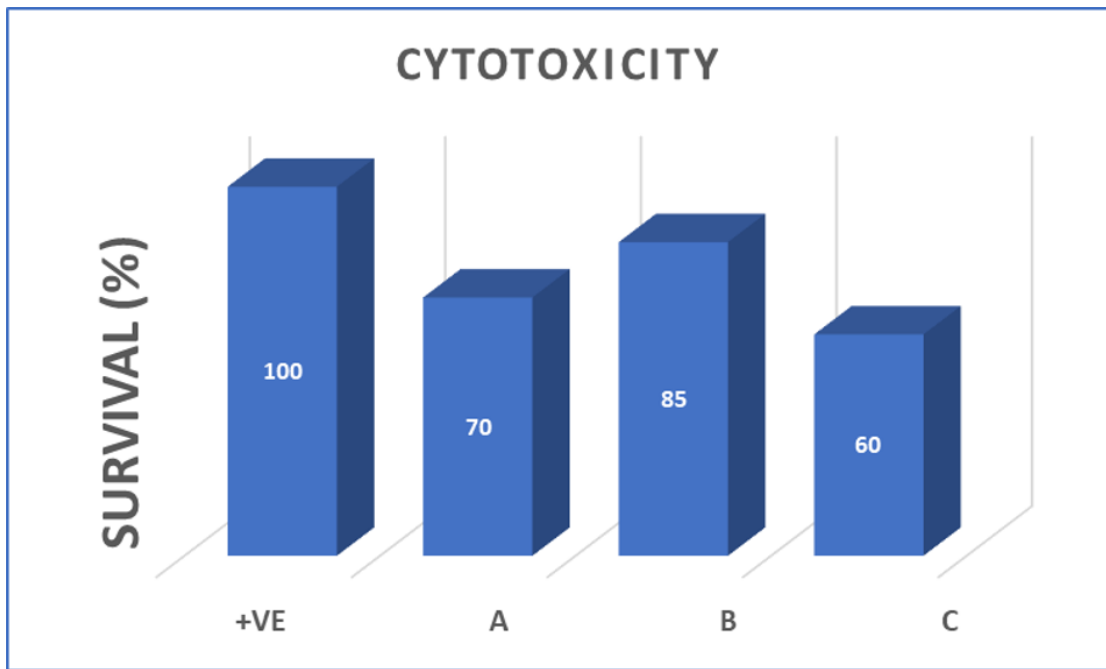


Figure 5.23: Image Of Cell Survival Percentage

5.2 Morphology of Nanofibers:

5.2.1 SEM:

In order to investigate the morphology of nanofibers, Scan Electron Microscope (SEM) analysis was performed on a sample of PICT/PAN core-shell nanofibers by using SEM (JSM-5300, JEOL Ltd., Japan) accelerated with the voltage of 12 kV as shown in **Figure 5.3**. It was observed that all PICT/PAN nanofibers prepared bead free and appreciable surface morphology. On the other hand, the size distribution study and the average nanofibers diameter was calculated by image J software, and it was analyzed that average diameter was not affected by the loading the CaO,SiO₂/HA ,ZnO NPs to PICT/PAN nanofibers. The average diameter of the nanofibers in absence of NPs was calculated to be about 375±40 nm. This amount changed to 250±18nm for 1st nanofabric, 300±25nm for 2nd nanofabric and 225±10 nm for 3rd nanofabric respectively . This indicates that nanofiber diameter was not changed by adding bioceramic NPs.

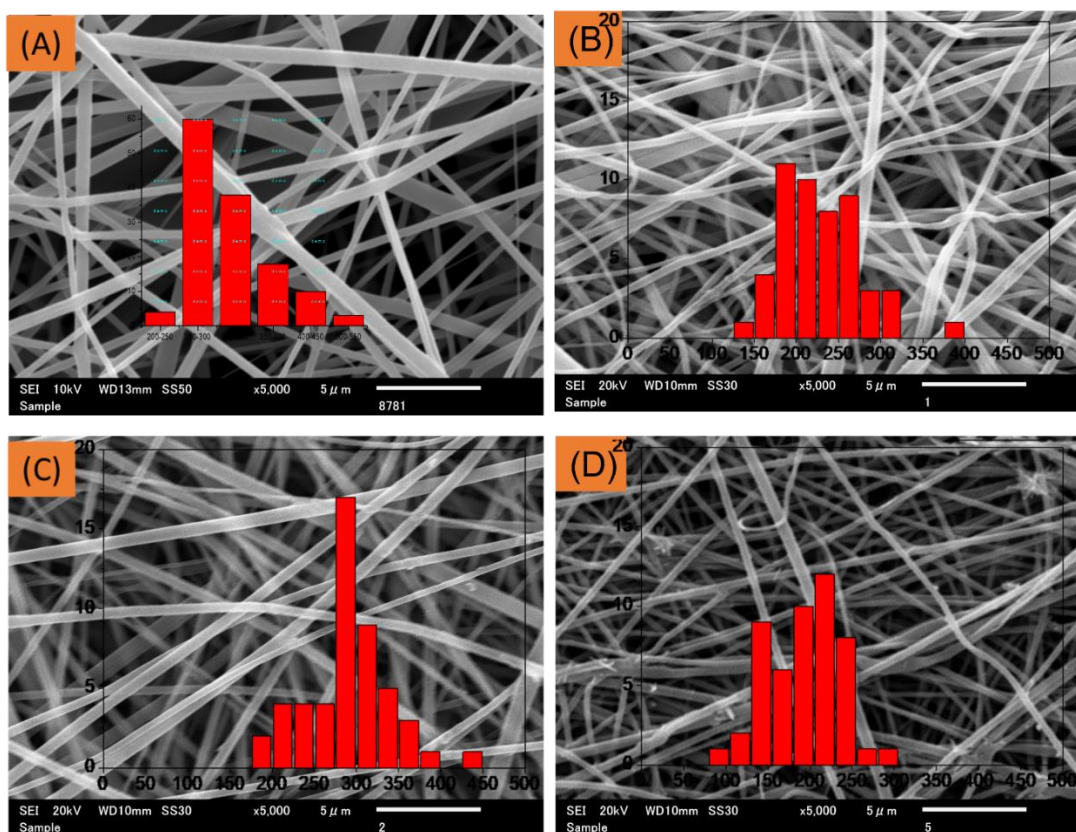


Figure 5.24: SEM Images of Nano Fibrous Scaffolds

5.2.2 TEM:

Transmission electron microscopy (TEM) analysis was performed using a JSM-5300 microscope (JEOL Ltd., Japan) with an acceleration voltage of 200 kV. The high-resolution TEM imaging allowed for detailed characterization of the nanofiber structure and the incorporation of suspended nanoparticles (NPs) within the fibers. By employing TEM imaging techniques, the present study provides important insights into the structural characteristics of the nanofiber-based drug delivery system.

In Figure 5.4, the core and shell regions of the nanofibers were clearly distinguishable due to their differential color densities. The outer light portion of each fiber corresponded to the sheath, while the centrally located dark part represented the core. This observation provided visual confirmation of the distinct core-shell structure of the fibers.

The NPs, serving as drug carriers, were intentionally incorporated into the core and shell solutions during the fabrication process. As the concentration of drug NPs increased from samples A to C, a corresponding increase in their presence within the

fibers was observed. The TEM analysis enabled the visualization and assessment of the distribution and extent of NP incorporation within the nanofiber matrix. This valuable information contributes to the understanding of how drugs are effectively incorporated into non-woven scaffold-based drug delivery systems. The TEM images demonstrate that the concentration of drug NPs plays a crucial role in determining their distribution within the fibers. This understanding has implications for optimizing drug loading strategies and controlling drug release kinetics in such systems.

The visualization of the core-shell structure and the incorporation of drug NPs within the fibers offer valuable knowledge for the development and design of advanced drug delivery platforms. These findings contribute to the field of biomedical engineering and can aid in the rational design of efficient and targeted drug delivery systems.

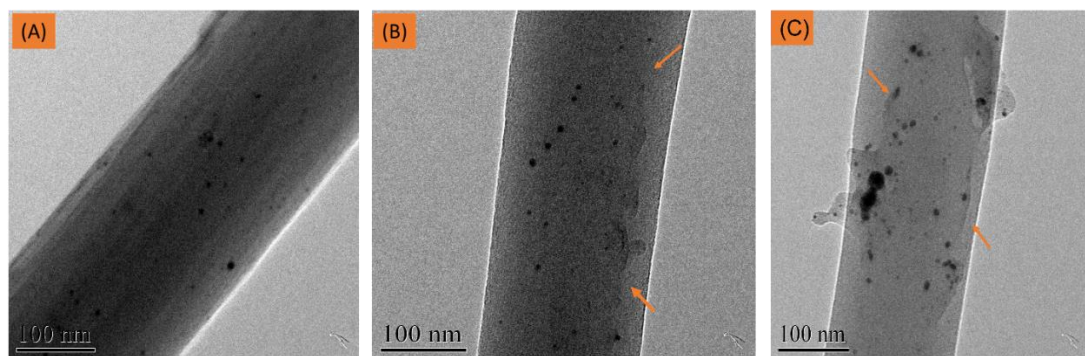


Figure 5.25: TEM Images of Scaffolds

5.3 Tensile Testing:

The stress-strain behavior of PICT/PAN nanofibers was investigated using a Universal Testing Machine (UTM) specifically the Tenilon RTC 250A (A&D Company Ltd., Japan). For each category of the samples, four specimens were prepared, maintaining an initial length of 26 mm and width of 2.8 mm. However, the thickness of the samples varied. The stress and strain values were calculated using the following formulas:

$$\text{Stress (S) in MPa} = \text{Average load values (N)} / \text{Area (m}^2\text{)}$$

$$\text{Strain (S) in MPa} = \text{Change in length } (\Delta l) / \text{Initial length (l)} \times 100$$

The results showed that the neat PICT electrospun nanofibers exhibited a highly profiled stress-strain behavior with a maximum tensile strength of 6 MPa compared to the other samples. However, it had a relatively low elongation of approximately 5%. On the other hand, sample C demonstrated the highest elongation but had a lower tensile strength or stress-bearing capacity compared to the other samples, as depicted in Figure 5.5. The reason behind the low tensile strength of sample C is attributed to its higher percentage of hydroxyapatite (HA) compared to the other samples, which is 6%. HA is known to be highly brittle and has a low Young's modulus, as reported in a study by Kumar, Dehiya [235].

Sample A exhibited a tensile strength of 2 MPa and an elongation of 7%, which was equivalent to sample B. If tensile strength was the ultimate design criterion, sample A would be the most suitable scaffold due to its favorable stress-bearing capacity and elongation. Sample B, however, emerged as a highly suitable scaffold that fulfilled both stated and implied requirements. It exhibited a stress-bearing capacity of approximately 1.5 MPa, which was appropriate, and an elongation of 7% in accordance with the requirements for scaffolds used in bone regeneration.

Furthermore, our scaffolds demonstrated higher tensile strength compared to a previous study on PVA/ZnO nanofabric membranes that aimed to increase membrane strength by increasing the ZnO content [236]. The PVA/ZnO nonwoven membranes with a maximum ZnO content of 9% exhibited a maximum tensile strength of 1.5 MPa. In contrast, scaffold A in our study, with 1.5% ZnO, achieved a tensile strength of 2 MPa, which is quite satisfactory for nonwoven scaffolds. These findings on the stress-strain behavior of the PICT/PAN nanofibers provide valuable insights into the mechanical properties of the scaffolds. The higher tensile strength and appropriate elongation exhibited by sample B make it a promising candidate for bone tissue engineering applications. This information contributes to the field of bone tissue engineering and assists in the design and optimization of scaffolds with enhanced mechanical performance for tissue engineering and regenerative purposes.

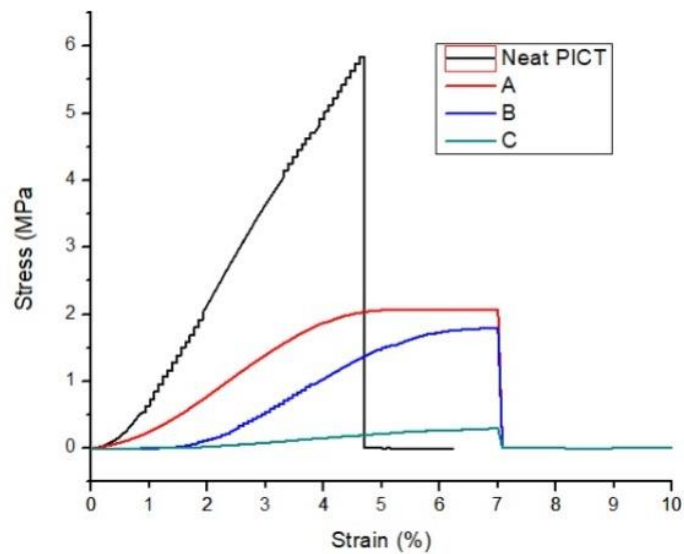


Figure 5.26: Tensile Strength and Elongation Graph

5.4 Water Contact Angle:

The wettability of the core and shell nanofibrous scaffold composed of poly(1,4-cyclohexanedimethylene isosorbide terephthalate) and PAN(Polyacrylonitrile) and loaded with [SiO₂-CaO/ZnO-HA] (Silicon dioxide-Calcium Oxide/Zinc Oxide-Hydroxyapatite) nanoparticles were assessed using an Optical Tensiometer. The evaluation of wettability using the Optical Tensiometer provides crucial insights into the interaction between the nanofiber scaffolds and water. This technique involved the careful placement of a water droplet on the surface of the samples using a micro-syringe, followed by capturing an image of the droplet on the surface and measuring the contact angle.

The results revealed important information about the wettability properties of the nanofibrous scaffolds. It was found that the neat PICT nanofibers exhibited the highest water contact angle, measuring 139.4°. This high contact angle indicated a highly hydrophobic nature of the neat PICT fibers, suggesting that they were less likely to absorb water and could maintain their structural integrity. In contrast, the blended 1st nanofibrous scaffold showed a contact angle of 125°, which was lower than the neat PICT fibers but still indicative of a hydrophobic nature. This suggested that the incorporation of the blended composite materials influenced the wettability of the scaffold. The 2nd nanofibrous scaffold demonstrated the highest and most

satisfactory water contact angle of 127.2° among all three composite nanofibers. This high contact angle value was highly desirable for bone scaffolds as it indicated a significant hydrophobic property. On the other hand, the 3rd scaffold, although highly hydrophobic, exhibited a slightly lower contact angle value of 120° compared to the 1st and 2nd scaffolds. This observation was depicted in Figure 5.6. It is worth noting that the increasing percentage of bioceramic nanoparticles in the composite scaffolds led to a decrease in the contact angle value. This trend of decreasing hydrophobicity could be attributed to the increased presence of amorphous regions within the scaffolds.

These findings have important implications for the design and development of bone scaffolds. The highly hydrophobic nature of the 2nd nanofibrous scaffold makes it a promising candidate for bone tissue engineering applications, as it can potentially repel water and maintain its mechanical strength in wet environments. However, the optimization of the composite composition and architecture should be carefully considered to balance hydrophobicity and other desired properties of the scaffold.

These findings contribute to the understanding of scaffold performance and aid in the design of effective tissue engineering platforms. Furthermore, the relationship between nanoparticle concentration and wettability offers valuable guidance for tailoring the properties of composite scaffolds for specific applications.

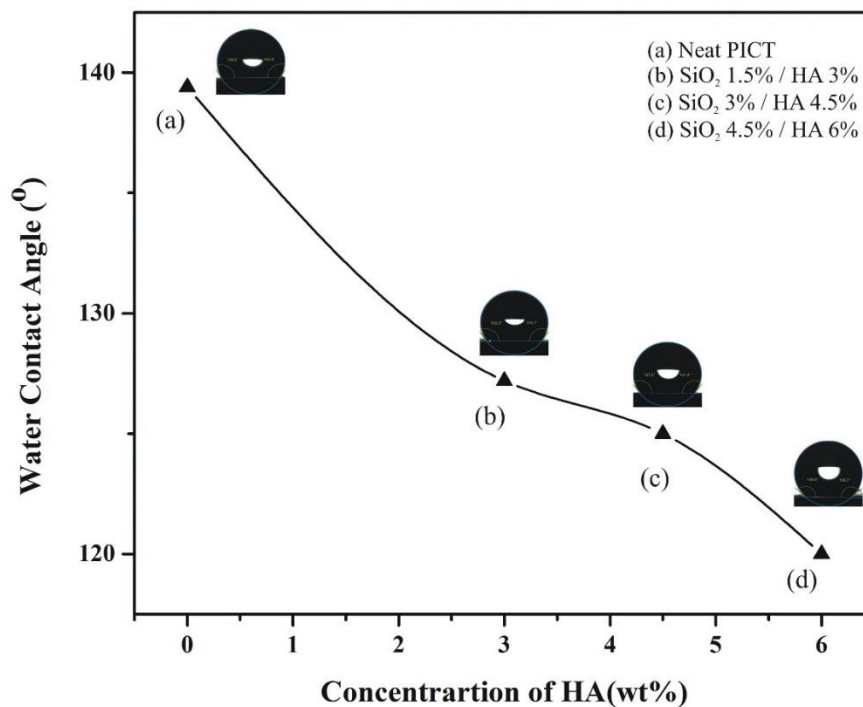


Figure 5.27: Graph Image of Wettability Behavior

5.5 FTIR Spectra:

The FTIR analysis of the scaffold's shell revealed important information about its composition and structure. A peak at 1238 cm^{-1} indicated the presence of C-O stretching vibrations in both cis and trans structures of poly (1,4-cyclohexane dimethylene isosorbide terephthalate) (PICT), confirming the incorporation of isosorbide units within the polymer backbone of the shell material. The inclusion of isosorbide units enhanced the material's mechanical strength, thermal stability, and biodegradability, making it suitable for tissue engineering and drug delivery applications. Another observation in the FTIR spectrum of the shell was the presence of Si-O-Si peaks at 1041 cm^{-1} , corresponding to the stretching vibrations of Si-O-Si bonds. These bonds provided structural integrity to the material by connecting the silicate-based moieties. The confirmation of this bonding motif supported the analysis of the shell's composition.

Moving to the scaffold's core, the FTIR analysis identified peaks at 2250 cm^{-1} and 2928 cm^{-1} , indicating the stretching vibrations associated with Polyacrylonitrile

(PAN). These peaks represented the $C\equiv N$ stretching mode, confirming the presence of nitrile groups ($-C\equiv N$) in PAN and its incorporation within the core structure. PAN contributed high strength, chemical resistance, and thermal stability to the scaffold, providing structural support and stability. Additionally, a peak at 572 cm^{-1} suggested the presence of zinc oxide (ZnO) in the core material. This peak corresponded to the stretching vibrations of Zn-O bonds, reflecting the connectivity and chemical composition of ZnO within the core. ZnO offered antimicrobial properties, UV protection, and piezoelectric behavior, potentially enhancing the functionalities of the core material. Furthermore, peaks at 3438 cm^{-1} and 1740 cm^{-1} indicated the stretching vibrations associated with hydroxyapatite. The peak at 3438 cm^{-1} represented the O-H stretching vibrations of hydroxyl groups ($-OH$) in hydroxyapatite, while the peak at 1740 cm^{-1} represented the stretching vibrations of $C=O$ bonds, indicating the presence of carbonate groups within the hydroxyapatite structure. These vibrational modes confirmed the incorporation of hydroxyapatite in the core and suggested its potential for biocompatibility and bone-regeneration capabilities.

FTIR analysis provided valuable insights into the composition and structural features of the scaffold's shell and core. The presence of specific stretching vibrations and bonding motifs elucidated the contributions of different functional groups to the material's properties. Understanding these characteristics is essential for utilizing scaffold in tissue engineering, drug delivery, and bone regeneration. It is important to note that the intensity variations in the FTIR spectra of scaffolds at different nanoparticle concentrations may have depended on various factors such as nanoparticle characteristics, scaffold matrix composition, and experimental conditions. A comprehensive analysis considering these factors is necessary to accurately interpret the intensity variations and their implications for the scaffold's composition and properties.

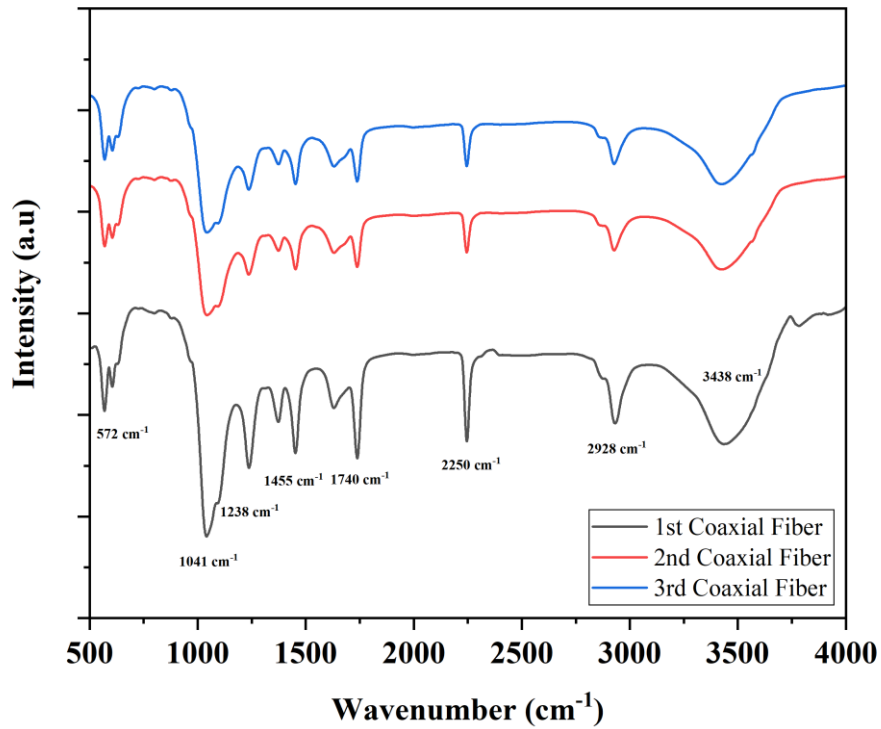


Figure 5.28: FTIR Spectra

5.6 FEM Results:

Upon performing the simulation as discussed in Chapter 4, the von Mises stress distribution was obtained, as depicted in Figure 5.8. This deformation analysis revealed that regions where the von Mises stress exceeded the fabric's ultimate tensile strength, leading to the development of necking regions. These localized areas of stress concentration occurred prior to complete failure, providing critical insights into the fabric's performance under tensile loading conditions.

0-14

0-15

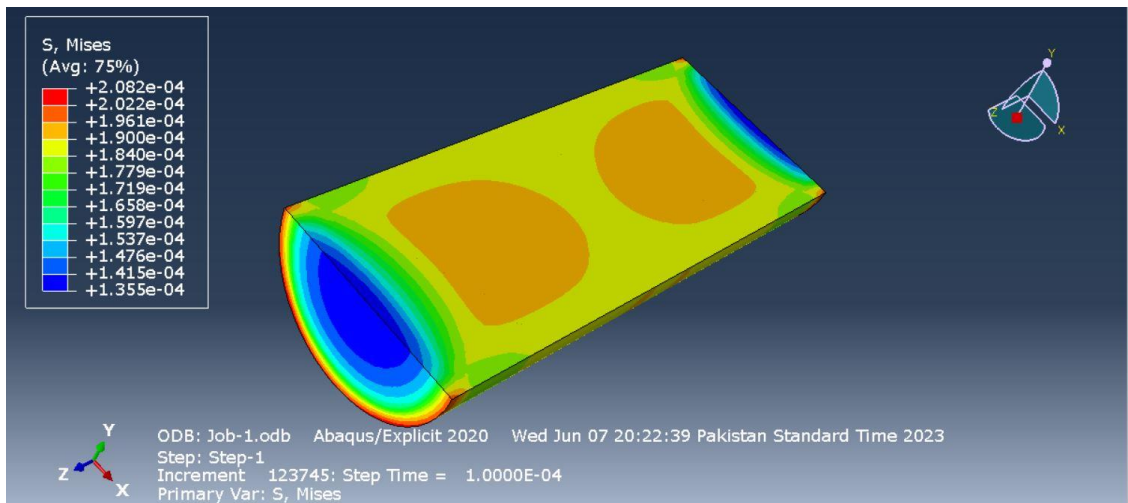


Figure 5.29

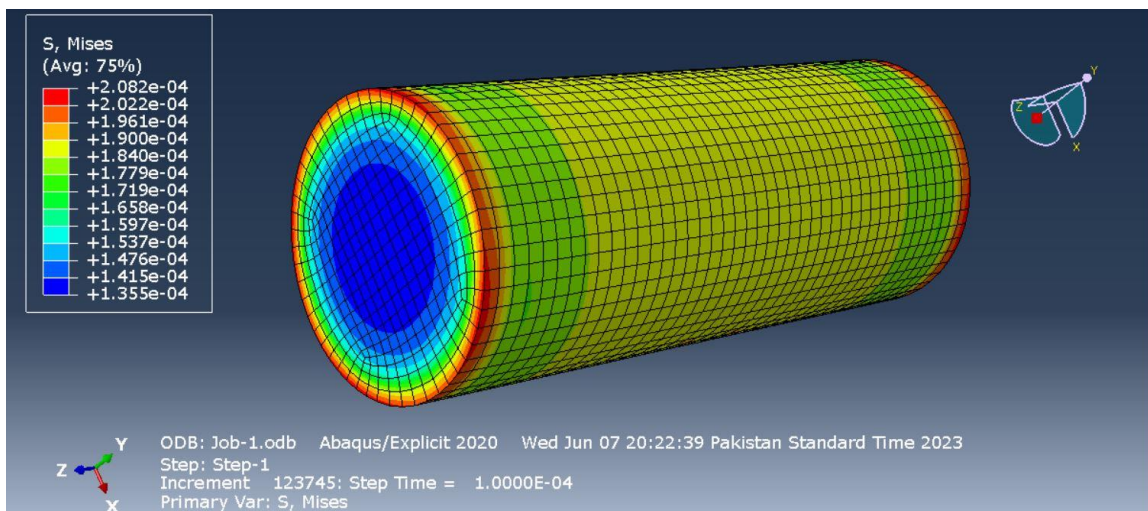


Figure 5.30

In addition to von Mises stress, the simulation also determined the maximum and minimum principal stresses within the fabric body. Figure 5.10 showcases these stress components, along with their respective direction vectors, further enhancing the understanding of stress distribution and potential failure mechanisms within the fabric.

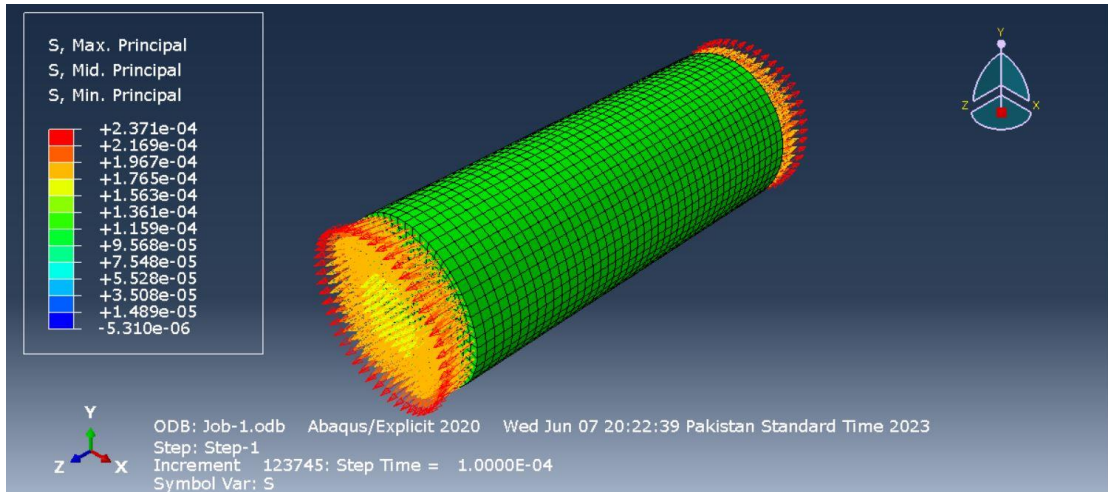


Figure 5.31: Stress Components Along Respective Direction Vectors

The results obtained from this comprehensive simulation and analysis provide valuable insights into the tensile behavior and failure mechanisms of the newly developed fabric. The knowledge gained from this study can serve as a foundation for further optimization and improvement of fabric design, ultimately contributing to the advancement of textile engineering and material science.

Conclusions

This comprehensive MS thesis focuses on the development of a non-woven coaxial nanofibrous polymeric scaffold for potential use in hard tissue engineering and regenerative applications. The study conducted is aimed at creating a controlled drug delivery system that can meet the required standards for bone regeneration applications.

In order to create an ideal scaffold with the desired properties, various scaffolding techniques such as electrospinning, bioprinting, and freeze drying were studied.

Electrospinning was selected as the method for fabricating the scaffold due to its advantages, including higher product selectivity, ability to draw coaxial nanofibers, cost-effectiveness, high production rate, simple process, more stable and a bone-compatible end product.

The scaffold is designed in such a way that every fiber has well defined core and shell. ZnO /HA and SiO₂ / CaO NPs were incorporated in core and shell of each fiber respectively.

To ensure the scaffold's mechanical stability, biocompatibility and physiochemical properties like hydrophobicity, the shell and core were constructed from biocompatible, non-toxic, high-strength and hydrophobic polymers PICT and PAN, respectively. The scaffold's mechanical properties were carefully studied, including its tensile strength, and elongation to ensure that it can withstand the stresses and provide support when implanted on bone.

Three scaffolds were fabricated with different percentages of bioceramic NPs used as drugs. To choose the most feasible scaffold many factors were put into consideration like structural properties, surface morphology, tensile strength, elongation before break, cell survival and wetting behavior.

After comparing all three scaffolds on the basis of above factors, it became evident that scaffold B was more feasible than the other two. The scaffold B showed excellent biocompatibility and supported the maximum survival of cells to 85% at the same time high resistance to wettability with water contact angle of 127.2° which is highly

desired to maintain the strength of scaffold that is responsible for guided bone regeneration. Scaffold B has a tensile strength of 1.7MPa and an elongation of 7%, which suggests that it has the potential to be used for guided bone regeneration. Scaffold A has a tensile strength of 2MPa, which is slightly higher than that of Scaffold B. However, both scaffolds have an equal elongation of 7%.

The study demonstrated that the scaffold's structure and properties, which includes the fiber diameter distribution, porosity, hydrophobicity, cell survival percentage and interconnectivity, is critical for its effectiveness in bone regeneration. The scaffold's structure influences its strength, the extent of cell infiltration, and the transportation of minerals and oxygen. Hence, the study optimized the electrospinning process to produce a scaffold with the desired structure.

In the end simulation of core and shell fiber was carried out by using ABAQUS software to analyze the behavior of single fiber under stress. In the near future we will use simulation to validate our experimental results and predict scaffold behavior with different compositions. This will optimize scaffold properties for specific applications and impact tissue regeneration.

Recommendations

The electrospun polymeric scaffold developed in this MS thesis has demonstrated great potential for use in tissue engineering and bone regeneration. Further studies can be conducted to optimize the scaffold's properties and test its effectiveness in vivo. With continued research and development, this scaffold can potentially be used in a wide range of applications in regenerative medicine and BTE.

The development of scaffolds for different body parts in regenerative medicine has unlocked immense potential for further research and advancements. Heart scaffolds have shown great promise in their ability to promote cardiac tissue regeneration and restore heart function, offering new avenues for treating cardiovascular diseases. Neural scaffolds hold the potential to revolutionize the treatment of nervous system injuries and disorders, opening doors to significant breakthroughs in neuroregeneration. Liver scaffolds, addressing the critical shortage of donor organs, present a remarkable opportunity to advance transplantation techniques and pave the way for the regeneration of functional liver tissue. Skin scaffolds, with their capability to facilitate the healing of burns, chronic wounds, and skin defects, hold tremendous potential for improving patient outcomes and quality of life. Additionally, cartilage scaffolds offer exciting prospects for effectively addressing cartilage-related conditions and injuries through tissue engineering approaches. The remarkable potential of scaffold research in these areas sets the stage for further research, innovation, and advancements in regenerative medicine to benefit countless patients in the future.

Scaffolds can be prepared for many other body parts, such as blood vessels, kidneys, lungs, and more. Advances in scaffold design, materials, and fabrication techniques continue to expand the possibilities for tissue regeneration and organ replacement in regenerative medicine.

References

- [1] Shier, D., J. Butler, and R. Lewis, *Hole's essentials of human anatomy & physiology*. 2012: McGraw-Hill New York, NY.
- [2] Arnold, C., *The skeletal system*. 2005: LernerClassroom.
- [3] Doherty, A.H., C.K. Ghalambor, and S.W.J.P. Donahue, *Evolutionary physiology of bone: bone metabolism in changing environments*. 2015. **30**(1): p. 17-29.
- [4] Shadjou, N. and M.J.J.o.B.M.R.P.A. Hasanzadeh, *Silica-based mesoporous nanobiomaterials as promoter of bone regeneration process*. 2015. **103**(11): p. 3703-3716.
- [5] Martins, A., R. Reis, and N.J.I.M.R. Neves, *Electrospinning: processing technique for tissue engineering scaffolding*. 2008. **53**(5): p. 257-274.
- [6] Pina, S., J.M. Oliveira, and R.L.J.A.M. Reis, *Natural-based nanocomposites for bone tissue engineering and regenerative medicine: A review*. 2015. **27**(7): p. 1143-1169.
- [7] Kretlow, J.D., L. Klouda, and A.G.J.A.d.d.r. Mikos, *Injectable matrices and scaffolds for drug delivery in tissue engineering*. 2007. **59**(4-5): p. 263-273.
- [8] Geraili, A., M. Xing, and K.J.V. Mequanint, *Design and fabrication of drug-delivery systems toward adjustable release profiles for personalized treatment*. 2021. **2**(5): p. 20200126.
- [9] Dimitriou, R., et al., *The role of barrier membranes for guided bone regeneration and restoration of large bone defects: current experimental and clinical evidence*. 2012. **10**: p. 1-24.
- [10] Keirouz, A., et al., *2D and 3D electrospinning technologies for the fabrication of nanofibrous scaffolds for skin tissue engineering: A review*. 2020. **12**(4): p. e1626.
- [11] Reneker, D., et al., *Electrospinning of nanofibers from polymer solutions and melts*. 2007. **41**: p. 43-346.
- [12] Bharadwaz, A., A.C.J.M.S. Jayasuriya, and E. C, *Recent trends in the application of widely used natural and synthetic polymer nanocomposites in bone tissue regeneration*. 2020. **110**: p. 110698.
- [13] Cui, W., et al., *Electrospun nanofibrous materials for tissue engineering and drug delivery*. 2010.

- [14] Prasad, S. and R.C.W.J.O.S.I. Wong, *Unraveling the mechanical strength of biomaterials used as a bone scaffold in oral and maxillofacial defects*. 2018. **15**(2): p. 48-55.
- [15] Thangavel, M., R.J.A.B.S. Elsen Selvam, and Engineering, *Review of Physical, Mechanical, and Biological Characteristics of 3D-Printed Bioceramic Scaffolds for Bone Tissue Engineering Applications*. 2022. **8**(12): p. 5060-5093.
- [16] Salgado, A.J., O.P. Coutinho, and R.L.J.M.b. Reis, *Bone tissue engineering: state of the art and future trends*. 2004. **4**(8): p. 743-765.
- [17] Yaszemski, M.J., et al., *Evolution of bone transplantation: molecular, cellular and tissue strategies to engineer human bone*. 1996. **17**(2): p. 175-185.
- [18] Deegan, A.J., *Novel tissue engineering approaches to enhance natural bone formation*. 2016, Keele University.
- [19] Buckwalter, J., et al., *Bone biology. I: Structure, blood supply, cells, matrix, and mineralization*. 1996. **45**: p. 371-386.
- [20] Chen, P.-Y., et al., *Minerals form a continuum phase in mature cancellous bone*. 2011. **88**(5): p. 351-361.
- [21] Junqueira, L., J. Carneiro, and R. Kelley, *Bone, basic histology*. 1995, Upper Saddle River, NJ: Prentice-Hall.
- [22] Barrere, F., et al., *Osteointegration of biomimetic apatite coating applied onto dense and porous metal implants in femurs of goats*. 2003. **67**(1): p. 655-665.
- [23] Birnbaum, K., et al., *Material properties of trabecular bone structures*. 2002. **23**(6): p. 399-407.
- [24] Thomas, N.C., *Incidence of Lower Limb Fractures among Rehabilitated Chronic Traumatic Spinal Cord injury patients at T10 Neurological Level and Below*. 2019, Christian Medical College, Vellore.
- [25] Maggiano, I.S., et al., *Three-dimensional reconstruction of Haversian systems in human cortical bone using synchrotron radiation-based micro-CT: morphology and quantification of branching and transverse connections across age*. 2016. **228**(5): p. 719-732.
- [26] Rey, C., et al., *Non-apatitic environments in bone mineral: FT-IR detection, biological properties and changes in several disease states*. 1989. **21**(1-4): p. 267-273.

- [27] Rey, C., et al., *The carbonate environment in bone mineral: a resolution-enhanced Fourier transform infrared spectroscopy study*. 1989. **45**(3): p. 157-164.
- [28] Cooper, R.R., J.W. MILGRAM, and R.A.J.J. ROBINSON, *Morphology of the osteon: an electron microscopic study*. 1966. **48**(7): p. 1239-1271.
- [29] Safadi, F.F., et al., *Bone structure, development and bone biology*. 2009: p. 1-50.
- [30] Blair, H.C., et al., *Osteoclastic bone resorption by a polarized vacuolar proton pump*. 1989. **245**(4920): p. 855-857.
- [31] Raja, I.S., et al., *Polyphenols-loaded electrospun nanofibers in bone tissue engineering and regeneration*. 2021. **25**: p. 1-16.
- [32] BERESFORD, J.N.J.C.O. and R. Research®, *Osteogenic stem cells and the stromal system of bone and marrow*. 1989. **240**: p. 270-280.
- [33] Taylor, J.J.B., *The periosteum and bone growth*. 1992. **6**: p. 21-52.
- [34] Vögelin, E., et al., *Healing of a critical-sized defect in the rat femur with use of a vascularized periosteal flap, a biodegradable matrix, and bone morphogenetic protein*. 2005. **87**(6): p. 1323-1331.
- [35] Muramatsu, K. and A.T.J.J.o.o.r. Bishop, *Cell repopulation in vascularized bone grafts*. 2002. **20**(4): p. 772-778.
- [36] Hutmacher, D.W. and M.J.T.e. Sittering, *Periosteal cells in bone tissue engineering*. 2003. **9**(4, Supplement 1): p. 45-64.
- [37] Epsley, S., et al., *The effect of inflammation on bone*. 2021. **11**: p. 1695.
- [38] Buckwalter, J., et al., *Bone biology. II: Formation, form, modeling, remodeling, and regulation of cell function*. 1996. **45**: p. 387-399.
- [39] Ferguson, C., et al., *Does adult fracture repair recapitulate embryonic skeletal formation?* 1999. **87**(1-2): p. 57-66.
- [40] Einhorn, T.A.J.C.O. and R. Research®, *The cell and molecular biology of fracture healing*. 1998. **355**: p. S7-S21.
- [41] Duvall, C.L., *The Role of Osteopontin in Postnatal Vascular Growth: Functional Effects in Ischemic Limb Collateral Vessel Formation and Long Bone Fracture Healing*. 2007, Georgia Institute of Technology.
- [42] McKibbin, B.J.T.J.o.b. and j.s.B. volume, *The biology of fracture healing in long bones*. 1978. **60**(2): p. 150-162.

- [43] Obert, L., F. Deschaseaux, and P.J.I. Garbuio, *Critical analysis and efficacy of BMPs in long bones non-union*. 2005. **36**(3): p. S38-S42.
- [44] Reddi, A.H.J.N.b., *Role of morphogenetic proteins in skeletal tissue engineering and regeneration*. 1998. **16**(3): p. 247-252.
- [45] Deckers, M.M., et al., *Bone morphogenetic proteins stimulate angiogenesis through osteoblast-derived vascular endothelial growth factor A*. 2002. **143**(4): p. 1545-1553.
- [46] Hoffmann, A., et al., *Perspectives in the biological function, the technical and therapeutic application of bone morphogenetic proteins*. 2001. **57**(3): p. 294-308.
- [47] Epari, D.R., et al., *Instability prolongs the chondral phase during bone healing in sheep*. 2006. **38**(6): p. 864-870.
- [48] *Osteochondral Defect Repair with Autologous Bone Marrow-Derived Mesenchymal Stem Cells in an Injectable, In Situ, Cross-Linked Synthetic Extracellular Matrix*. 2006. **12**(12): p. 3405-3416.
- [49] Lienau, J., et al., *Initial vascularization and tissue differentiation are influenced by fixation stability*. 2005. **23**(3): p. 639-645.
- [50] Urist, M.R.J.S., *Bone: formation by autoinduction*. 1965. **150**(3698): p. 893-899.
- [51] Wozney, J.M., et al., *Novel regulators of bone formation: molecular clones and activities*. 1988. **242**(4885): p. 1528-1534.
- [52] Nakashima, M. and A.H.J.N.b. Reddi, *The application of bone morphogenetic proteins to dental tissue engineering*. 2003. **21**(9): p. 1025-1032.
- [53] Bessa, P.C., et al., *Bone morphogenetic proteins in tissue engineering: the road from the laboratory to the clinic, part I (basic concepts)*. 2008. **2**(1): p. 1-13.
- [54] Lieberman, J.R., A. Daluiski, and T.A.J.J. Einhorn, *The role of growth factors in the repair of bone: biology and clinical applications*. 2002. **84**(6): p. 1032-1044.
- [55] Schmitt, J.M., et al., *Bone morphogenetic proteins: an update on basic biology and clinical relevance*. 1999.
- [56] Tsuji, K., et al., *BMP2 activity, although dispensable for bone formation, is required for the initiation of fracture healing*. 2006. **38**(12): p. 1424-1429.

- [57] Reddi, A.H.J.C.O. and R. Research®, *Initiation of fracture repair by bone morphogenetic proteins*. 1998. **355**: p. S66-S72.
- [58] Amédée, J., et al., *Osteogenin (bone morphogenetic protein 3) inhibits proliferation and stimulates differentiation of osteoprogenitors in human bone marrow*. 1995. **58**(2): p. 157-164.
- [59] Lecanda, F., L.V. Avioli, and S.L.J.J.o.c.b. Cheng, *Regulation of bone matrix protein expression and induction of differentiation of human osteoblasts and human bone marrow stromal cells by bone morphogenetic protein-2*. 1997. **67**(3): p. 386-398.
- [60] Obri, A., et al., *Osteocalcin in the brain: from embryonic development to age-related decline in cognition*. *Nature Reviews Endocrinology*, 2018. **14**(3): p. 174-182.
- [61] Fiedler, J., et al., *BMP-2, BMP-4, and PDGF-bb stimulate chemotactic migration of primary human mesenchymal progenitor cells*. 2002. **87**(3): p. 305-312.
- [62] Mishima, Y. and M.J.J.o.O.R. Lotz, *Chemotaxis of human articular chondrocytes and mesenchymal stem cells*. 2008. **26**(10): p. 1407-1412.
- [63] Bostrom, M.P., N.P.J.C.O. Camacho, and R. Research, *Potential role of bone morphogenetic proteins in fracture healing*. 1998. **355**: p. S274-S282.
- [64] Bostrom, M.P., et al., *Immunolocalization and expression of bone morphogenetic proteins 2 and 4 in fracture healing*. 1995. **13**(3): p. 357-367.
- [65] Onishi, T., et al., *Distinct and overlapping patterns of localization of bone morphogenetic protein (BMP) family members and a BMP type II receptor during fracture healing in rats*. 1998. **22**(6): p. 605-612.
- [66] Ronga, M., et al., *Clinical applications of growth factors in bone injuries: experience with BMPs*. 2013. **44**: p. S34-S39.
- [67] MacKenzie, E.J., et al., *Long-term persistence of disability following severe lower-limb trauma: results of a seven-year follow-up*. 2005. **87**(8): p. 1801-1809.
- [68] Borrelli, J., et al., *Treatment of nonunions and osseous defects with bone graft and calcium sulfate*. 2003. **411**: p. 245-254.
- [69] Starr, A.J.J.J., *Fracture repair: successful advances, persistent problems, and the psychological burden of trauma*. 2008. **90**(Supplement_1): p. 132-137.

- [70] Laurencin, C., Y. Khan, and S.F.J.E.r.o.m.d. El-Amin, *Bone graft substitutes*. 2006. **3**(1): p. 49-57.
- [71] Simon Jr, C.G., et al., *Preliminary report on the biocompatibility of a moldable, resorbable, composite bone graft consisting of calcium phosphate cement and poly (lactide-co-glycolide) microspheres*. 2002. **20**(3): p. 473-482.
- [72] Cypher, T.J., J.P.J.T.J.o.f. Grossman, and a. surgery, *Biological principles of bone graft healing*. 1996. **35**(5): p. 413-417.
- [73] Praemer, A., S. Furner, and D.J.R. Rice, IL, *Musculoskeletal conditions in the United States; American Academy of Orthopaedic Surgeons*. 1999: p. 182.
- [74] Giannoudis, P.V., H. Dinopoulos, and E.J.I. Tsiridis, *Bone substitutes: an update*. 2005. **36**(3): p. S20-S27.
- [75] Younger, E.M. and M.W.J.J.O.T. Chapman, *Morbidity at bone graft donor sites*. 1989. **3**(3): p. 192-195.
- [76] Arrington, E.D., et al., *Complications of iliac crest bone graft harvesting*. 1996. **329**: p. 300-309.
- [77] Prolo, D.J., J.J.J.C.O. Rodrigo, and R. Research, *Contemporary bone graft physiology and surgery*. 1985. **200**: p. 322-342.
- [78] Wheeler, D.L., W.F.J.C.O. Enneking, and R. Research, *Allograft bone decreases in strength in vivo over time*. 2005. **435**: p. 36-42.
- [79] Govender, S., et al., *Recombinant human bone morphogenetic protein-2 for treatment of open tibial fractures: a prospective, controlled, randomized study of four hundred and fifty patients*. 2002. **84**(12): p. 2123-2134.
- [80] Papakostidis, C., et al., *Efficacy of autologous iliac crest bone graft and bone morphogenetic proteins for posterolateral fusion of lumbar spine: a meta-analysis of the results*. 2008. **33**(19): p. E680-E692.
- [81] Friedlaender, G.E., et al., *Osteogenic protein-1 (bone morphogenetic protein-7) in the treatment of tibial nonunions: a prospective, randomized clinical trial comparing rhOP-1 with fresh bone autograft*. 2001. **83**(Pt 2): p. S151.
- [82] Kanakaris, N.K., et al., *Application of BMP-7 to tibial non-unions: a 3-year multicenter experience*. 2008. **39**: p. S83-S90.
- [83] Cahill, K.S., et al., *Prevalence, complications, and hospital charges associated with use of bone-morphogenetic proteins in spinal fusion procedures*. 2009. **302**(1): p. 58-66.

- [84] Benglis, D., M.Y. Wang, and A.D.J.O.N. Levi, *A comprehensive review of the safety profile of bone morphogenetic protein in spine surgery*. 2008. **62**(suppl_5): p. ONS423-ONS431.
- [85] Dahabreh, Z., et al., *A cost analysis of treatment of tibial fracture nonunion by bone grafting or bone morphogenetic protein-7*. 2009. **33**: p. 1407-1414.
- [86] Garrison, K.R., et al., *Clinical effectiveness and cost-effectiveness of bone morphogenetic proteins in the non-healing of fractures and spinal fusion: a systematic review*. 2007. **11**(30): p. 1-150, iii.
- [87] Rose, F.R., R.O.J.B. Oreffo, and b.r. communications, *Bone tissue engineering: hope vs hype*. 2002. **292**(1): p. 1-7.
- [88] Tabata, Y.J.T.e., *Tissue regeneration based on growth factor release*. 2003. **9**(4, Supplement 1): p. 5-15.
- [89] Parenteau, N.J.S.A., *Skin: the first tissue-engineered products*. 1999. **280**(4): p. 83-85.
- [90] Gemmiti, C.V. and R.E.J.T.e. Guldberg, *Fluid flow increases type II collagen deposition and tensile mechanical properties in bioreactor-grown tissue-engineered cartilage*. 2006. **12**(3): p. 469-479.
- [91] Lima, E.G., et al., *Functional tissue engineering of chondral and osteochondral constructs*. 2004. **41**(3-4): p. 577-590.
- [92] Porter, B.D., et al., *Noninvasive image analysis of 3D construct mineralization in a perfusion bioreactor*. 2007. **28**(15): p. 2525-2533.
- [93] Pelled, G., et al., *Direct gene therapy for bone regeneration: gene delivery, animal models, and outcome measures*. 2010. **16**(1): p. 13-20.
- [94] Kempen, D.H., et al., *Effect of local sequential VEGF and BMP-2 delivery on ectopic and orthotopic bone regeneration*. 2009. **30**(14): p. 2816-2825.
- [95] Oest, M.E., et al., *Quantitative assessment of scaffold and growth factor-mediated repair of critically sized bone defects*. 2007. **25**(7): p. 941-950.
- [96] Nerem, R.M.J.T.e., *Tissue engineering: the hope, the hype, and the future*. 2006. **12**(5): p. 1143-1150.
- [97] Guldberg, R.E.J.J.o.B. and M. Research, *Spatiotemporal delivery strategies for promoting musculoskeletal tissue regeneration*. 2009. **24**(9): p. 1507-1511.
- [98] Guldberg, R., et al., *Biologic augmentation of polymer scaffolds for bone repair*. 2007. **7**(4): p. 333.

- [99] Patterson, T.E., et al., *Cellular strategies for enhancement of fracture repair*. 2008. **90**(Supplement_1): p. 111-119.
- [100] Giannoudis, P.V., et al., *The diamond concept—open questions*. 2008. **39**: p. S5-S8.
- [101] Gamradt, S.C. and J.R.J.A.o.b.e. Lieberman, *Genetic modification of stem cells to enhance bone repair*. 2004. **32**: p. 136-147.
- [102] Phillips, J.E., et al., *Mineralization capacity of Runx2/Cbfa1-genetically engineered fibroblasts is scaffold dependent*. 2006. **27**(32): p. 5535-5545.
- [103] Petrie, T.A., et al., *Simple application of fibronectin–mimetic coating enhances osseointegration of titanium implants*. 2009. **13**(8b): p. 2602-2612.
- [104] Friess, W., et al., *Bone regeneration with recombinant human bone morphogenetic protein-2 (rhBMP-2) using absorbable collagen sponges (ACS): influence of processing on ACS characteristics and formulation*. 1999. **4**(3): p. 387-396.
- [105] Hosseinkhani, H., et al., *Osteogenic differentiation of mesenchymal stem cells in self-assembled peptide-amphiphile nanofibers*. 2006. **27**(22): p. 4079-4086.
- [106] Lee, J.-Y., et al., *Osteoblastic differentiation of human bone marrow stromal cells in self-assembled BMP-2 receptor-binding peptide-amphiphiles*. 2009. **30**(21): p. 3532-3541.
- [107] Malafaya, P.B., G.A. Silva, and R.L.J.A.d.d.r. Reis, *Natural–origin polymers as carriers and scaffolds for biomolecules and cell delivery in tissue engineering applications*. 2007. **59**(4-5): p. 207-233.
- [108] Hutmacher, D.W., et al., *Mechanical properties and cell cultural response of polycaprolactone scaffolds designed and fabricated via fused deposition modeling*. 2001. **55**(2): p. 203-216.
- [109] Lin, A.S., et al., *Microarchitectural and mechanical characterization of oriented porous polymer scaffolds*. 2003. **24**(3): p. 481-489.
- [110] Dean, D., et al., *Poly (propylene fumarate) and poly (DL-lactic-co-glycolic acid) as scaffold materials for solid and foam-coated composite tissue-engineered constructs for cranial reconstruction*. 2003. **9**(3): p. 495-504.
- [111] Murugan, R. and S.J.T.e. Ramakrishna, *Nano-featured scaffolds for tissue engineering: a review of spinning methodologies*. 2006. **12**(3): p. 435-447.

- [112] Chu, T.-M.G., et al., *Segmental bone regeneration using a load-bearing biodegradable carrier of bone morphogenetic protein-2*. 2007. **28**(3): p. 459-467.
- [113] Meinig, R.J.I., *Poly lactide membranes in the treatment of segmental diaphyseal defects: animal model experiments in the rabbit radius, sheep tibia, Yucatan minipig radius, and goat tibia*. 2002. **33**: p. 58-65.
- [114] Gugala, Z. and S.J.I. Gogolewski, *Healing of critical-size segmental bone defects in the sheep tibiae using bioresorbable polylactide membranes*. 2002. **33**: p. 71-76.
- [115] Giardino, R., et al., *Bioabsorbable scaffold for in situ bone regeneration*. 2006. **60**(8): p. 386-392.
- [116] Jung, U.-W., et al., *Effects of a chitosan membrane coated with polylactic and polyglycolic acid on bone regeneration in a rat calvarial defect*. 2007. **2**(3): p. S101.
- [117] Kim, K.-H., et al., *Biological efficacy of silk fibroin nanofiber membranes for guided bone regeneration*. 2005. **120**(3): p. 327-339.
- [118] Matthews, J.A., et al., *Electrospinning of collagen nanofibers*. 2002. **3**(2): p. 232-238.
- [119] Pham, Q.P., U. Sharma, and A.G.J.T.e. Mikos, *Electrospinning of polymeric nanofibers for tissue engineering applications: a review*. 2006. **12**(5): p. 1197-1211.
- [120] Lee, K.Y. and D.J.J.C.r. Mooney, *Hydrogels for tissue engineering*. 2001. **101**(7): p. 1869-1880.
- [121] Lutolf, M.P., et al., *Synthetic matrix metalloproteinase-sensitive hydrogels for the conduction of tissue regeneration: engineering cell-invasion characteristics*. 2003. **100**(9): p. 5413-5418.
- [122] Bruder, S.P., B.S.J.C.O. Fox, and R. Research, *Tissue engineering of bone: cell based strategies*. 1999. **367**: p. S68-S83.
- [123] Hunziker, E.B.J.O. and cartilage, *Articular cartilage repair: basic science and clinical progress. A review of the current status and prospects*. 2002. **10**(6): p. 432-463.
- [124] Song, L., D. Baksh, and R.J.C. Tuan, *Mesenchymal stem cell-based cartilage tissue engineering: cells, scaffold and biology*. 2004. **6**(6): p. 596-601.

- [125] Bruder, S.P., et al., *The effect of implants loaded with autologous mesenchymal stem cells on the healing of canine segmental bone defects*. 1998. **80**(7): p. 985-96.
- [126] Bruder, S.P., et al., *Bone regeneration by implantation of purified, culture-expanded human mesenchymal stem cells*. 1998. **16**(2): p. 155-162.
- [127] Kadiyala, S., et al., *Culture expanded canine mesenchymal stem cells possess osteochondrogenic potential in vivo and in vitro*. 1997. **6**(2): p. 125-134.
- [128] McCulloch, C., et al., *Osteogenic progenitor cells in rat bone marrow stromal populations exhibit self-renewal in culture*. 1991. **77**(9): p. 1906-1911.
- [129] Banfi, A., et al., *Replicative aging and gene expression in long-term cultures of human bone marrow stromal cells*. 2002. **8**(6): p. 901-910.
- [130] Quarto, R., D. Thomas, and C.J.C.t.i. Liang, *Bone progenitor cell deficits and the age-associated decline in bone repair capacity*. 1995. **56**: p. 123-129.
- [131] D'ippolito, G., et al., *Age-related osteogenic potential of mesenchymal stromal stem cells from human vertebral bone marrow*. 1999. **14**(7): p. 1115-1122.
- [132] De Coppi, P., et al., *Isolation of amniotic stem cell lines with potential for therapy*. 2007. **25**(1): p. 100-106.
- [133] Peister, A., et al., *Osteogenic differentiation of amniotic fluid stem cells*. 2008. **18**(4): p. 241.
- [134] Kolambkar, Y.M., et al., *Chondrogenic differentiation of amniotic fluid-derived stem cells*. 2007. **38**: p. 405-413.
- [135] Gersbach, C.A., et al., *Runx2/Cbfa1-genetically engineered skeletal myoblasts mineralize collagen scaffolds in vitro*. 2004. **88**(3): p. 369-378.
- [136] Ishaug-Riley, S.L., et al., *Three-dimensional culture of rat calvarial osteoblasts in porous biodegradable polymers*. 1998. **19**(15): p. 1405-1412.
- [137] Byers, B.A., R.E. Guldborg, and A.J.J.T.e. García, *Synergy between genetic and tissue engineering: Runx2 overexpression and in vitro construct development enhance in vivo mineralization*. 2004. **10**(11-12): p. 1757-1766.
- [138] Cartmell, S., et al., *Quantitative microcomputed tomography analysis of mineralization within three-dimensional scaffolds in vitro*. 2004. **69**(1): p. 97-104.
- [139] Thorrez, L., et al., *Growth, differentiation, transplantation and survival of human skeletal myofibers on biodegradable scaffolds*. 2008. **29**(1): p. 75-84.

- [140] Jäger, M., et al., *Bone healing and migration of cord blood—derived stem cells into a critical size femoral defect after xenotransplantation*. 2007. **22**(8): p. 1224-1233.
- [141] Zhang, X., et al., *Periosteal progenitor cell fate in segmental cortical bone graft transplantations: implications for functional tissue engineering*. 2005. **20**(12): p. 2124-2137.
- [142] Cooley, J.F., *Apparatus for electrically dispersing fluids*. 1902, Google Patents.
- [143] Rayleigh, L.J.T.L., Edinburgh,, D.P. Magazine, and J.o. Science, XX. *On the equilibrium of liquid conducting masses charged with electricity*. 1882. **14**(87): p. 184-186.
- [144] Anton, F., *Method and apparatus for spinning*. 1939, Google Patents.
- [145] Anton, F., *Artificial thread and method of producing same*. 1940, Google Patents.
- [146] Taylor, G.I.J.P.o.t.R.S.o.L.A.M. and P. Sciences, *Electrically driven jets*. 1969. **313**(1515): p. 453-475.
- [147] Taylor, G.I.J.P.o.t.R.S.o.L.S.A.M. and P. Sciences, *Disintegration of water drops in an electric field*. 1964. **280**(1382): p. 383-397.
- [148] Baumgarten, P.K.J.J.o.c. and i. science, *Electrostatic spinning of acrylic microfibers*. 1971. **36**(1): p. 71-79.
- [149] Larrondo, L. and R.J.J.o.P.S.P.P.E. St. John Manley, *Electrostatic fiber spinning from polymer melts. I. Experimental observations on fiber formation and properties*. 1981. **19**(6): p. 909-920.
- [150] Larrondo, L. and R.J.J.o.P.S.P.P.E. St. John Manley, *Electrostatic fiber spinning from polymer melts. II. Examination of the flow field in an electrically driven jet*. 1981. **19**(6): p. 921-932.
- [151] Annis, D., et al., *An elastomeric vascular prosthesis*. 1978. **24**(1): p. 209-214.
- [152] Fisher, A., et al., *Long term in-vivo performance of an electrostatically-spun small bore arterial prosthesis: the contribution of mechanical compliance and anti-platelet therapy*. 1985. **3**: p. 462-465.
- [153] Doshi, J. and D.H.J.J.o.e. Reneker, *Electrospinning process and applications of electrospun fibers*. 1995. **35**(2-3): p. 151-160.
- [154] Boys, C.V.J.P.o.t.P.S.o.L., *On the production, properties, and some suggested uses of the finest threads*. 1887. **9**(1): p. 8.

- [155] Liu, S. and D.H.J.P. Reneker, *Droplet-jet shape parameters predict electrospun polymer nanofiber diameter*. 2019. **168**: p. 155-158.
- [156] Sun, B.J.P.P.S., Long Y. Zhang H. Li M. Duvail J. Jiang X. Yin H. 2014. **39**: p. 862-890.
- [157] Xue, J., et al., *Electrospinning and electrospun nanofibers: Methods, materials, and applications*. 2019. **119**(8): p. 5298-5415.
- [158] Jiang, S., et al., *Unusual and superfast temperature-triggered actuators*. 2015. **27**(33): p. 4865-4870.
- [159] Min, L.-L., et al., *Preparation of chitosan based electrospun nanofiber membrane and its adsorptive removal of arsenate from aqueous solution*. 2015. **267**: p. 132-141.
- [160] Lee, J.K.Y., et al., *Polymer-based composites by electrospinning: Preparation & functionalization with nanocarbons*. 2018. **86**: p. 40-84.
- [161] Liu, M., et al., *A review: electrospun nanofiber materials for lithium-sulfur batteries*. 2019. **29**(49): p. 1905467.
- [162] Zhang, C.-L. and S.-H.J.M.H. Yu, *Spraying functional fibres by electrospinning*. 2016. **3**(4): p. 266-269.
- [163] Wu, H., et al., *Electrospinning of ceramic nanofibers: Fabrication, assembly and applications*. 2012. **1**(1): p. 2-23.
- [164] Schiffman, J. and C. Schauer, *A review: electrospinning of biopolymer nanofibers and their applications*. *Polym Rev* 48: 317–352. 2008.
- [165] Liao, Y., et al., *Progress in electrospun polymeric nanofibrous membranes for water treatment: Fabrication, modification and applications*. 2018. **77**: p. 69-94.
- [166] Luo, C., et al., *Electrospinning versus fibre production methods: from specifics to technological convergence*. 2012. **41**(13): p. 4708-4735.
- [167] Ren, L.-F., et al., *Experimental investigation of the effect of electrospinning parameters on properties of superhydrophobic PDMS/PMMA membrane and its application in membrane distillation*. 2017. **404**: p. 155-166.
- [168] Haider, A., S. Haider, and I.-K.J.A.J.o.C. Kang, *A comprehensive review summarizing the effect of electrospinning parameters and potential applications of nanofibers in biomedical and biotechnology*. 2018. **11**(8): p. 1165-1188.

- [169] Zeng, J., et al., *Poly-L-lactide nanofibers by electrospinning—Influence of solution viscosity and electrical conductivity on fiber diameter and fiber morphology*. *e-Polym.* 2003; 1; 3 (1). DOI.
- [170] Demir, M.M., et al., *Electrospinning of polyurethane fibers*. 2002. **43**(11): p. 3303-3309.
- [171] Deitzel, J.M., et al., *The effect of processing variables on the morphology of electrospun nanofibers and textiles*. 2001. **42**(1): p. 261-272.
- [172] Sill, T.J. and H.A.J.B. Von Recum, *Electrospinning: applications in drug delivery and tissue engineering*. 2008. **29**(13): p. 1989-2006.
- [173] Garg, K. and G.L.J.B. Bowlin, *Electrospinning jets and nanofibrous structures*. 2011. **5**(1): p. 013403.
- [174] Yarin, A.L., S. Koombhongse, and D.H.J.J.o.a.p. Reneker, *Bending instability in electrospinning of nanofibers*. 2001. **89**(5): p. 3018-3026.
- [175] Zhao, Y., et al., *Study on correlation of morphology of electrospun products of polyacrylamide with ultrahigh molecular weight*. 2005. **43**(16): p. 2190-2195.
- [176] Yang, Q., et al., *Influence of solvents on the formation of ultrathin uniform poly (vinyl pyrrolidone) nanofibers with electrospinning*. 2004. **42**(20): p. 3721-726.
- [177] Yarin, A.L., S. Koombhongse, and D.H.J.J.o.a.p. Reneker, *Taylor cone and jetting from liquid droplets in electrospinning of nanofibers*. 2001. **90**(9): p. 4836-4846.
- [178] Lannutti, J., et al., *Electrospinning for tissue engineering scaffolds*. 2007. **27**(3): p. 504-509.
- [179] Liu, Z., et al., *Electrospun jets number and nanofiber morphology effected by voltage value: numerical simulation and experimental verification*. 2019. **14**(1): p. 1-9.
- [180] Lee, J.S., et al., *Role of molecular weight of atactic poly (vinyl alcohol)(PVA) in the structure and properties of PVA nanofabric prepared by electrospinning*. 2004. **93**(4): p. 1638-1646.
- [181] Buchko, C.J., et al., *Processing and microstructural characterization of porous biocompatible protein polymer thin films*. 1999. **40**(26): p. 7397-7407.
- [182] Wu, C.M., et al., *Effects of electrostatic polarity and the types of electrical charging on electrospinning behavior*. 2012. **126**(S2): p. E89-E97.

- [183] Matabola, K. and R.J.J.o.M.S. Moutloali, *The influence of electrospinning parameters on the morphology and diameter of poly (vinylidene fluoride) nanofibers-effect of sodium chloride*. 2013. **48**(16): p. 5475-5482.
- [184] Ding, W., et al., *Manipulated electrospun PVA nanofibers with inexpensive salts*. 2010. **295**(10): p. 958-965.
- [185] Beachley, V., X.J.M.S. Wen, and E. C, *Effect of electrospinning parameters on the nanofiber diameter and length*. 2009. **29**(3): p. 663-668.
- [186] Zargham, S., et al., *The effect of flow rate on morphology and deposition area of electrospun nylon 6 nanofiber*. 2012. **7**(4): p. 155892501200700414.
- [187] Gao, J., et al., *Electrically conductive and fluorine free superhydrophobic strain sensors based on SiO₂/graphene-decorated electrospun nanofibers for human motion monitoring*. 2019. **373**: p. 298-306.
- [188] Chen, S.-H., et al., *A three-dimensional dual-layer nano/microfibrous structure of electrospun chitosan/poly (D, L-lactide) membrane for the improvement of cytocompatibility*. 2014. **450**: p. 224-234.
- [189] Chang, W.-M., C.-C. Wang, and C.-Y.J.E.A. Chen, *Fabrication of ultra-thin carbon nanofibers by centrifuged-electrospinning for application in high-rate supercapacitors*. 2019. **296**: p. 268-275.
- [190] Megelski, S., et al., *Micro-and nanostructured surface morphology on electrospun polymer fibers*. 2002. **35**(22): p. 8456-8466.
- [191] Pelipenko, J., et al., *The impact of relative humidity during electrospinning on the morphology and mechanical properties of nanofibers*. 2013. **456**(1): p. 125-134.
- [192] Park, J.-Y., I.-H.J.J.o.n. Lee, and nanotechnology, *Relative humidity effect on the preparation of porous electrospun polystyrene fibers*. 2010. **10**(5): p. 3473-3477.
- [193] Huan, S., et al., *Effect of experimental parameters on morphological, mechanical and hydrophobic properties of electrospun polystyrene fibers*. 2015. **8**(5): p. 2718-2734.
- [194] De Vrieze, S., et al., *The effect of temperature and humidity on electrospinning*. 2009. **44**: p. 1357-1362.
- [195] Teo, W.E. and S.J.N. Ramakrishna, *A review on electrospinning design and nanofibre assemblies*. 2006. **17**(14): p. R89.

- [196] Katta, P., et al., *Continuous electrospinning of aligned polymer nanofibers onto a wire drum collector*. 2004. **4**(11): p. 2215-2218.
- [197] Bhattarai, N., et al., *Electrospun chitosan-based nanofibers and their cellular compatibility*. 2005. **26**(31): p. 6176-6184.
- [198] Teimouri, A., M.J.I.J.o.P.M. Azadi, and P. Biomaterials, *Preparation and characterization of novel chitosan/nanodiopside/nanohydroxyapatite composite scaffolds for tissue engineering applications*. 2016. **65**(18): p. 917-927.
- [199] Schwarzenbach, M.S., et al., *Interferon α -2a interactions on glass vial surfaces measured by atomic force microscopy*. 2002. **56**(2): p. 78-89.
- [200] Zhang, B., et al., *3D bioprinting: a novel avenue for manufacturing tissues and organs*. 2019. **5**(4): p. 777-794.
- [201] Ngo, T.J.C.P.B.-e., A. kashani, G. imbalzano, k. Nguyen, d. hui. 2018. **143**: p. 172-196.
- [202] Bishop, E.S., et al., *3-D bioprinting technologies in tissue engineering and regenerative medicine: Current and future trends*. 2017. **4**(4): p. 185-195.
- [203] Munaz, A., et al., *Three-dimensional printing of biological matters*. 2016. **1**(1): p. 1-17.
- [204] Hu, W., et al., *Advances in crosslinking strategies of biomedical hydrogels*. 2019. **7**(3): p. 843-855.
- [205] Fahimipour, F., et al., *Enhancing cell seeding and osteogenesis of MSCs on 3D printed scaffolds through injectable BMP2 immobilized ECM-Mimetic gel*. 2019. **35**(7): p. 990-1006.
- [206] Mancha Sánchez, E., et al., *Hydrogels for bioprinting: A systematic review of hydrogels synthesis, bioprinting parameters, and bioprinted structures behavior*. 2020. **8**: p. 776.
- [207] Obregon, F., et al., *Three-Dimensional Bioprinting for Regenerative Dentistry and Craniofacial Tissue Engineering*. *Journal of Dental Research*, 2015. **94**(9_suppl): p. 143S-152S.
- [208] Zhang, Y.S., et al., *Bioprinting 3D microfibrinous scaffolds for engineering endothelialized myocardium and heart-on-a-chip*. 2016. **110**: p. 45-59.
- [209] Pourchet, L.J., et al., *Human skin 3D bioprinting using scaffold-free approach*. 2017. **6**(4): p. 1601101.

- [210] Michael, S., et al., *Tissue engineered skin substitutes created by laser-assisted bioprinting form skin-like structures in the dorsal skin fold chamber in mice*. 2013. **8**(3): p. e57741.
- [211] Gu, Q., et al., *Functional 3D neural mini-tissues from printed gel-based bioink and human neural stem cells*. 2016. **5**(12): p. 1429-1438.
- [212] Malone, E. and H.J.R.P.J. Lipson, *Fab@ Home: the personal desktop fabricator kit*. 2007. **13**(4): p. 245-255.
- [213] Smith, C.M., et al., *Three-dimensional bioassembly tool for generating viable tissue-engineered constructs*. 2004. **10**(9-10): p. 1566-1576.
- [214] Yan, Y., et al., *Layered manufacturing of tissue engineering scaffolds via multi-nozzle deposition*. 2003. **57**(18): p. 2623-2628.
- [215] Ozbolat, I.T. and Y.J.I.T.o.B.E. Yu, *Bioprinting toward organ fabrication: challenges and future trends*. 2013. **60**(3): p. 691-699.
- [216] Dababneh, A.B., I.T.J.J.o.M.S. Ozbolat, and Engineering, *Bioprinting technology: a current state-of-the-art review*. 2014. **136**(6).
- [217] Koch, L., et al., *Laser printing of skin cells and human stem cells*. 2010. **16**(5): p. 847-854.
- [218] Rider, P., et al., *Bioprinting of tissue engineering scaffolds*. 2018. **9**: p. 2041731418802090.
- [219] Murphy, S.V., A. Skardal, and A.J.J.o.B.M.R.P.A. Atala, *Evaluation of hydrogels for bio-printing applications*. 2013. **101**(1): p. 272-284.
- [220] Costa, J.B., et al., *3D bioprinted highly elastic hybrid constructs for advanced fibrocartilaginous tissue regeneration*. 2020. **32**(19): p. 8733-8746.
- [221] Huebner, K.H., et al., *The finite element method for engineers*. 2001: John Wiley & Sons.
- [222] BAKKER, A., A.H. Haidari, and L.M.J.C.e.p. Oshinowo, *Realize greater benefits from CFD*. 2001. **97**(3): p. 45-53.
- [223] Surana, K., et al., *k-version of finite element method in gas dynamics: Higher-order global differentiability numerical solutions*. 2007. **69**(6): p. 1109-1157.
- [224] Gravenkamp, H., C. Birk, and C.J.J.o.c.p. Song, *Simulation of elastic guided waves interacting with defects in arbitrarily long structures using the scaled boundary finite element method*. 2015. **295**: p. 438-455.
- [225] Liu, Y. and N.J.E.A.w.B.E. Nishimura, *The fast multipole boundary element method for potential problems: a tutorial*. 2006. **30**(5): p. 371-381.

- [226] Veronese, F.M., et al., *PEG–Doxorubicin Conjugates: Influence of Polymer Structure on Drug Release, in Vitro Cytotoxicity, Biodistribution, and Antitumor Activity*. *Bioconjugate Chemistry*, 2005. **16**(4): p. 775-784.
- [227] Aydin, H.M., et al., *Study of tissue engineered bone nodules by Fourier transform infrared spectroscopy*. 2011. **136**(4): p. 775-780.
- [228] Paschalis, E.P., et al., *Infrared assessment of bone quality: a review*. 2011. **469**: p. 2170-2178.
- [229] Miller, L.M., et al., *Accretion of bone quantity and quality in the developing mouse skeleton*. 2007. **22**(7): p. 1037-1045.
- [230] Young, T.J.P.t.o.t.r.s.o.L., III. *An essay on the cohesion of fluids*. 1805(95): p. 65-87.
- [231] Karbowiak, T., et al., *Importance of surface tension characterization for food, pharmaceutical and packaging products: A review*. 2006. **46**(5): p. 391-407.
- [232] Solaro, R., F. Chiellini, and A.J.M. Battisti, *Targeted delivery of protein drugs by nanocarriers*. 2010. **3**(3): p. 1928-1980.
- [233] Kiritchenko, S., et al. *NRC-Canada-2014: Detecting aspects and sentiment in customer reviews*. in *Proceedings of the 8th international workshop on semantic evaluation (SemEval 2014)*. 2014.
- [234] Akhtar, K., et al., *Scanning electron microscopy: Principle and applications in nanomaterials characterization*. 2018: p. 113-145.
- [235] Kumar, P., B.S. Dehiya, and A.J.I.J.A.E.R. Sindhu, *Bioceramics for hard tissue engineering applications: A review*. 2018. **13**(5): p. 2744-2752.
- [236] Khan, M.Q., et al., *Preparation and characterizations of multifunctional PVA/ZnO nanofibers composite membranes for surgical gown application*. 2019. **8**(1): p. 1328-1334.

